Accepted Manuscript

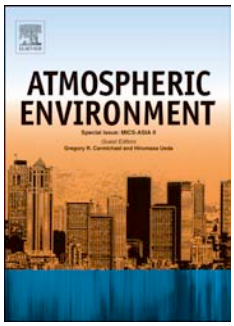

Impacts of future climate and emission changes on U.S. air quality

Ashley Penrod, Yang Zhang, Kai Wang, Shiang-Yuh Wu, L. Ruby Leung

PII: S1352-2310(14)00002-8

DOI: 10.1016/j.atmosenv.2014.01.001

Reference: AEA 12679

To appear in: *Atmospheric Environment*

Received Date: 21 October 2013

Revised Date: 27 December 2013

Accepted Date: 1 January 2014

Please cite this article as: Penrod, A., Zhang, Y., Wang, K., Wu, S.-Y., Leung, L.R., Impacts of future climate and emission changes on U.S. air quality, *Atmospheric Environment* (2014), doi: 10.1016/j.atmosenv.2014.01.001.

Highlights:

(1) Comprehensive evaluation of latest CMAQ v5.0 for multi-years (2001-2005)
(2) Responses of future air quality/deposition to climate and emission changes
(3) Anthropogenic emission reduction dominates future $PM_{2.5}$ levels

Impacts of Future Climate and Emission Changes on U.S. Air Quality

Ashley Penrod[a], Yang Zhang[a,*], Kai Wang[a], Shiang-Yuh Wu[b], and L. Ruby Leung[c]

[a]Department of Marine, Earth, and Atmospheric Sciences, North Carolina State University, Raleigh, North Carolina, USA.
[b]Department of Air Quality and Environmental Management, Clark County, Nevada, USA.
[c]Pacific Northwest National Laboratory, Richland, Washington, USA.

*Corresponding author: Yang Zhang, Department of MEAS, NCSU, Campus Box 8208, Raleigh, NC 27695-8208, USA. Tel: 919 515 9688; fax: 919 515 7802. Email address: yang_zhang@ncsu.edu

ABSTRACT

Changes in climate and emissions will affect future air quality. In this work, simulations of regional air quality during current (2001-2005) and future (2026-2030) winter and summer are conducted with the newly released CMAQ version 5.0 to examine the impacts of simulated future climate and anthropogenic emission projections on air quality over the U.S. Current meteorological and chemical predictions are evaluated against observations to assess the model's capability in reproducing the seasonal differences. WRF and CMAQ capture the overall observational spatial patterns and seasonal differences. Biases in model predictions are attributed to uncertainties in emissions, boundary conditions, and limitations in model physical and chemical treatments as well as the use of a coarse grid resolution. Increased temperatures (up to 3.18 °C) and decreased ventilation (up to 157 m in planetary boundary layer height) are found in both future winter and summer, with more prominent changes in winter. Increases in future temperatures result in increased isoprene and terpene emissions in winter and summer, driving the increase in maximum 8-h average O_3 (up to 5.0 ppb) over the eastern U.S. in winter while decreases in NO_x emissions drive the decrease in O_3 over most of the U.S. in summer. Future $PM_{2.5}$ concentrations in winter and summer and many of its components decrease due to decreases in primary anthropogenic emissions and the concentrations of secondary anthropogenic pollutants as well as increased precipitation in winter. Future winter and summer dry and wet deposition fluxes are spatially variable and increase with decreasing surface resistance and precipitation, respectively. They decrease with a decrease in ambient particulate concentrations. Anthropogenic emissions play a more important role in summer than in winter for future O_3 and $PM_{2.5}$ levels, with a dominance of the effects of significant emission reductions over those of climate change on future $PM_{2.5}$ levels.

KEYWORDS: Future climate change, emissions, air quality, CMAQ, WRF, model evaluation

1. Introduction

Future projections of regional air quality must account for changes in both future emissions and climate due to their closely-coupled impacts on air quality. Major air pollutants, such as ozone (O_3) and particulate matter (PM), are sensitive to many meteorological parameters including temperature, relative humidity, precipitation, wind speed, and mixing height, making it imperative

that the relationship between meteorology and air quality be examined. The relationship between air quality and emissions is also important, as increases in the emissions of primary air pollutants and the precursors of secondary pollutants will lead to air pollution thus poor air quality.

The influence of climate and/or emissions on future air quality has been extensively studied, particularly the influence on surface O_3 and PM. Among past studies, some included the impact of climate change (including biogenic emissions) on future air quality (e.g., Zhang et al. 2008; Jacob and Winner, 2009; Weaver et al., 2009; Fiore et al., 2011; Manders et al., 2012; Tai et al., 2012), some included the impact of projected anthropogenic emissions on future air quality (e.g., S. Wu et al., 2008a; Zhang et al. 2010a; Stevenson et al., 2012), and some included changes in both climate change and anthropogenic emissions (e.g., Hogrefe et al. 2004; Unger et al., 2006; Tagaris et al., 2007; S. Wu et al., 2008a, b; Nolte et al., 2008; and Lam et al., 2011; Stevenson et al., 2012; Young et al., 2012; Lei et al., 2012; Doherty et al., 2013; Gao et al., 2013). As an example of combined impact of climate change and anthropogenic emissions, Tagaris et al. (2007) simulated changes in future air quality in the United States (U.S.) due to climate change and emission reductions and found 9% and 23% decrease in 2050 mean summer maximum 8-hr average O_3 and mean annual PM with aerodynamic diameters less than or equal to 2.5 μm ($PM_{2.5}$), respectively. Some of the studies on future air quality assess the separate and combined impact of future climate and emission projections. For example, S. Wu et al. (2008b) reported an increase of maximum 8-hr average O_3 by 2-15 ppb in the U.S. by 2050 due to climate change alone and a decrease by 1-5 ppb in the western U.S. and 5-15 ppb in the eastern U.S. due to anthropogenic emission projections based on the IPCC A1B scenario. Lam et al. (2011) showed a similar range of results for maximum 8-hr average O_3 and a decrease of annual average $PM_{2.5}$ by 40% to 50%, with 10% of the impact due to climate change and 90% due to projected anthropogenic emission changes.

Although the effects of emissions have been shown as a major driver of future air quality (e.g., S. Wu et al., 2008a, b; Zhang et al., 2010a; Lam et al., 2011), the impact of climate change

cannot be ignored as it can offset the impacts of anthropogenic emission reductions. Increased temperature and net radiative flux can increase concentrations of most air pollutants such as O_3 by accelerating the rates of photochemical reactions, while decreased wind speed (WS) at a receptor and decreased planetary boundary layer height (PBLH) at any location can increase concentrations due to decreased dispersion and ventilation. Increased precipitation at any location and increased WS at a source can cleanse the atmosphere of pollutants through scavenging and dispersion. Increased temperatures and radiation, decreased cloud cover, and reduced precipitation as reported in Leung and Gustafson (2005) will likely increase future maximum 8-h average O_3 mixing ratios, particularly on the east coast, and decrease surface concentrations of $PM_{2.5}$ over much of the U.S. (Zhang et al., 2008). Dawson et al. (2009) suggested a 1.7 ppb increase in grid average maximum 8-h average O_3 over the U.S. for July 2050 due to increased temperature and decreases wind speed and mixing height, but predicted a decrease over the Northeast. Hogrefe et al. (2004) reported a domain wide mean increase in maximum 8-h average O_3 mixing ratios for July of 2020, 2050, and 2080 by 2.7, 4.2, and 5.0 ppb, respectively, but found that the O_3 increases did not spatially correlate with any one specific meteorological variable. This demonstrates that atmospheric chemical reactions and transport processes are complex and nonlinear, which may differ among studies and result in spatial and qualitative differences in model predictions of future air quality due to the impact of climate.

The objectives of this study are to estimate future climate, emissions, and air quality trends and to assess the combined contributions of climate change and anthropogenic emission projections on regional air quality over the U.S. This work is distinguished from previous studies that have included the impacts of both climate and emission changes in several aspects. First, previous studies used either an older version of the Community Multiscale Air Quality (CMAQ) (e.g., Hogrefe et al., 2004; Tagaris et al., 2007; Zhang et al., 2008;) or other models (e.g., Jacob and Winner, 2009; Pye et al., 2009; Lei et al., 2012; Doherty et al., 2013), while this study uses the

newly released CMAQ version 5.0 that contains updated model treatments for several processes (see section 2.1). Only one study (i.e., Gao et al., 2013) used CMAQ version 5.0 but it only focused on the impact of future changes in climate and emissions on O_3 and did not include the impact on $PM_{2.5}$. Second, for meteorological fields, most of the previous work used MM5 (e.g., Tagaris et al., 2007; Dawson et al., 2009), whereas this work uses the Weather Research and Forecasting (WRF) model version 3.2. It has been shown in previous studies that WRF performs similar to MM5 and, for some variables, better than MM5 (Appel et al., 2010; Gilliam and Pleim, 2010). Third, previous studies included limited model evaluation and/or focused on a single or ≤ 3 years (or season/month), whereas this work includes a comprehensive, 5-year (i.e., 2001-2005) assessment in terms of both meteorological and chemical predictions. For the year 2002, model simulation with meteorological conditions driven by the reanalysis data from the National Center of Environmental Prediction (NCEP) are evaluated to show the baseline model skill when driven by more realistic large-scale conditions from global reanalysis.

2. Model configuration, observational data sets, and evaluation protocol

2.1 Model setup and inputs

The pre-released beta version (as of summer 2011) of the U.S. Environmental Protection Agency (EPA)'s latest version of the CMAQ modeling system (Byun and Schere, 2006), version 5.0 is used in this work, which was publically released in February 2012 (CMAQ 5.0 release note at http://cmascenter.org/cmaq/; Appel et al., 2013). Table S1 in the supplementary material shows the model configurations. Chemical initial and lateral boundary conditions (ICs and BCs) are based on the Goddard Earth Observing System Model with Chemistry (GEOS-Chem) 2002 output (Bey et al., 2001) and are kept constant for all current/future year simulations.

Meteorological fields for all baseline and sensitivity simulations are generated using WRF version 3.2 (Skamarock et al., 2008). Two sets of WRF simulations are performed: one for the current (2001-2005) and future (2026-2030) climate (referred to as WRF_CCSM) and another for

model evaluation for one current year (2002; referred to as WRF_NCEP). There are two major differences between WRF_CCSM and WRF_NCEP. First, ICs and BCs for the WRF_CCSM simulations are initialized at the beginning of the simulation, run for 5.5-day and reinitialized every 5 days with the first 0.5 day discarded as model spinup, and driven by CCSM dataset at the lateral boundaries every 6 hours to capture the large-scale climatology of the future and current years, while the WRF_NCEP simulation is initialized with and driven by the NCEP-Final (NCEP-FNL) Operational Global Analysis data to better replicate the current large-scale atmospheric conditions. Second, four-dimensional data assimilation (FDDA) is used to constrain the u- and v-components of wind, temperature, and specific humidity in both WRF_CCSM and WRF_NCEP simulations by the large-scale conditions from CCSM and NCEP, respectively. However, the u- and v-components are nudged in the PBL and above for the WRF_NCEP simulations following Stauffer et al. (1991) and only nudged above the PBL in the WRF_CCSM simulations. Differences in the simulation setup allow each simulation to better capture the observed meteorological conditions with the respective lateral boundary forcing. The Meteorological Chemistry Interface Processor (MCIP) version 4.0 is used to post-process all WRF output into CMAQ readable I/O API formatted files.

Criteria and hazardous air pollutant emission inventories and ancillary files for current year simulations are based on the U.S. EPA's 2002 National Emissions Inventory (NEI), while biogenic emissions for both current and future year scenarios are processed in-line with CMAQ v5.0 and are based on the Biogenic Emissions Inventory System (BEIS) version 3.13. Domain-wide speciated growth factors for future (2026-2030) anthropogenic emissions are applied to the base 2002 NEI speciated, model-ready, and gridded emissions. The future-year simulations are based on the IPCC SRES A1B scenario, which is characterized by rapid economic growth, moderate population growth that peaks in 2050 and declines thereafter, and rapid growth and introduction of new, more energy efficient technologies, with a balance across all energy sectors (IPCC, 2000). Table S2 shows the lumped growth factors (GFs) for the A1B scenario that are derived based on GFs for 8

source sectors over the U.S. developed by Argonne National Laboratory (ANL) (personal communications, David Streets, ANL, 2011). These growth factors are applied to the gridded 2002 NEI emissions to produce the gridded future year emissions inventory.

The baseline and sensitivity simulations cover the contiguous U.S. including portions of southern Canada and northern Mexico, and are conducted at a horizontal grid resolution of 36 km and a vertical resolution of 14 layers from the surface to about 15 km (~100 mb). Baseline simulations are conducted for summer (June, July, August (JJA)) and winter (December, January, February (DJF)) of 5 current years (2001-2005) and 5 future years (2026-2030). Changes in simulated meteorological and chemical variables as well as biogenic emissions are estimated by calculating the difference between the average future (2026-2030) and current years (2001-2005).

To understand the impact of projected anthropogenic emission changes on future air quality, sensitivity simulations (Sen) are conducted for representative winters and summers in which future anthropogenic emissions are kept the same as those in 2002. To reduce computational requirements, four sets of simulations are completed to examine a range of possible impacts from interannual variability of the future meteorological conditions; one summer and one winter where future climate may lead to poor air quality and one summer and one winter where future climate may lead to improved air quality. Meteorological conditions that may lead to poor air quality with increased pollutant concentrations include decreased precipitation (Precip), cloud fraction (CFRAC), and PBLH and increased temperature and shortwave radiation reaching the ground (GSW), while the opposite holds for improved air quality. By comparing individual winter and summer during 2026-2030 with the 5-year average of 2026-2030 in terms of meteorological parameters that affect air quality, the summer and winter of 2029 are chosen as poor and good air quality seasons, respectively, while the summer of 2030 is chosen as a good air quality summer, and the winter of 2026 is a poor air quality winter. The relative contribution of anthropogenic emissions alone on air quality will also be examined by taking the difference between the baseline

simulations of the corresponding years (i.e., summer 2029 and 2030 and winter 2029 and 2026, which include both anthropogenic emissions and climate changes (Baseline), and the Sen simulation (which include only changes in climate; e.g., Baseline 2029 – Sen 2029).

2.2 Observational datasets and evaluation protocols

Observational datasets used to compare with the WRF/CMAQ simulations are obtained from a number of observational networks and satellites as summarized in Table S3. Meteorological variables to be evaluated include temperature at 2-m (T2), water vapor mixing ratio at 2 m (QV2), relative humidity at 2-m (RH2), precipitation (Precip), wind speed at 10-m (WS10), wind direction at 10-m (WD10), and Precip. The simulated PBLHs are also analyzed. These are the most influential meteorological variables for atmospheric chemical reactions and the transport of many pollutants. Air quality variables examined include maximum 1-h and 8-h average O_3, mixing ratios of carbon monoxide (CO), NO_2 (nitrogen dioxide), SO_2 (sulfur dioxide), HNO_3 (nitric acid), and NH_3 (ammonia), $PM_{2.5}$ and its components (i.e., sulfate (SO_4^{2-}), nitrate (NO_3^-), ammonium (NH_4^+), organic carbon (OC), and elemental carbon (EC)), wet and dry deposition fluxes of SO_4^{2-}, NH_4^+, and NO_3^-, as well as visibility parameters (extinction coefficient (β_{ext}) and haziness index (HI)). Surface-based observations are obtained from nine monitoring networks: the Clean Air Status and Trends Network (CASTNET), the Aerometric Information Retrieval System-Air Quality System (AIRS-AQS), the Interagency Monitoring of Protected Visual Environments (IMPROVE), the Chemical Speciation Network (CSN), the Southeastern Aerosol Research and Characterization study (SEARCH), the North Carolina Department of Environment and Natural Resources (NCDENR), and the National Acid Deposition Program (NADP). In addition, the model's ability to capture the column mass abundances of CO, NO_2, O_3, HCHO, and AOD are also evaluated using satellite measurements, which are described in the supplementary material.

Meteorological and chemical predictions for summer (JJA) and winter (DJF) of 2002 from WRF_NCEP/CMAQ v5.0 are compared to all available observations in 2002 through a

191 comprehensive evaluation. In addition, meteorological and chemical predictions for summer and
192 winter of 2001-2005 from WRF_CCSM/CMAQ v5.0 are compared to observations over a 5-yr
193 average (i.e., average of 2001-2005). Spatial, statistical, and column abundance comparisons of
194 WRF_NCEP/CMAQ simulations and observations are conducted, using a set of performance
195 statistic metrics recommended by Seigneur et al. (2000) and Zhang et al. (2006, 2009a). The
196 statistic metrics used include normalized mean bias (NMB), normalized mean error (NME), and
197 correlation coefficient (Corr) for both spatial and temporal distributions. Although WRF/CMAQ
198 with NCEP and CCSM initialization and boundary conditions are obtained through different means
199 (i.e., derived from reanalysis and a general circulation model (GCM), respectively), their simulated
200 spatial distribution trends in meteorological variables and chemical compositions are overall similar
201 for summer and winter (figures not shown), indicating that CCSM is able to capture the
202 climatological features of the NCEP reanalysis. To further verify the representativeness of the
203 simulations driven by CCSM for 2001-2005, statistical evaluation of meteorological and chemical
204 predictions against observations with the WRF_CCSM/CMAQ v5.0 simulations is conducted.
205 Evaluation of WRF_NCEP/CMAQ v5.0 and WRF_CCSM/CMAQ v5.0 (with the exception of
206 Precip, NH_3, visibility parameters, and column abundance) is performed with the U.S. EPA's
207 Atmospheric Model Evaluation Tool (AMET) (Appel et al., 2011a).

208 **3. Evaluation of model performance under current year conditions**

209 **3.1 Meteorological predictions**

210 WRF and CMAQ are evaluated for the base year winter and summer to assess the models'
211 ability to capture seasonal trends in current years before their applications for future climate and air
212 quality predictions. Table 1 summarizes the seasonal statistical performance of WRF_NCEP
213 meteorological predictions. T2 is generally well reproduced in terms of NMBs and NMEs when
214 compared to observations from different networks (with the exception of winter at SEARCH sites),
215 with a range of -18.7% to 4.2% for NMB, 7.4-34.0% for NME, and 0.7-1.0 for Corr for both

seasons. The relatively large cold biases in winter (e.g., -1.6 °C at the CSN sites and -3.9 °C at SEARCH sites) may be due to too cold soil initial temperatures and inappropriate snow treatments as well as limitations in the PBL scheme (under more stable conditions), land-surface model, and radiation schemes in current meteorological models (Gilliam et al., 2006; Zhang et al., 2010b). RH2 is overpredicted in winter with NMBs of 11.3-19.1%, but are better predicted in the summer with NMBs ranging from -1.3% to 4%. Overpredictions occur for WS10 at all sites, particularly at the CASTNET sites in winter and summer (NMBs of 50.3% and 48.8%, respectively). A large bias of WS10 has been a persistent problem associated with all PBL schemes in WRF and may be due to the variance of terrain and/or unresolved subgrid-scale topographic features, and uncertainties in parameterizations of turbulent fluxes (Hanna and Yang, 2001; Rontu, 2006; Mass and Ovens, 2011). Seasonal-mean precipitation over the domain is moderately underestimated in winter (with an NMB of -33.2%), but largely overpredicted in the summer (with an NMB of 65.9%), which will impact chemical predictions, including gas-phase and particulate concentrations and wet and total deposition fluxes. The biases of Precip may be due to limitations of the land-surface, cumulus, and microphysics schemes used in the simulation, as well as the missing subgrid-scale cloud feedbacks in WRF as suggested by Alapaty et al. (2012). These results for summer 2002 are similar to or better than those of Zhang et al. (2012), who performed a WRF/Chem simulation of July 2001 over the continental U.S. and reported NMBs of -3.9% to 2.9% for T2, NMBs of -15.0% to -5.1% for RH2, NMBs of 49.0-98.4% for WS10, and NMBs of 53.0-55.6% for Precip. The improved statistical performance for some meteorological variables in this work compared to Zhang et al. (2012) may be related to the use of FDDA that constrains the simulated large-scale circulation to be close to that of the reanalysis throughout the model domain and a newer version of WRF (v3.2 vs. v3.0) with some updates and bug fixes in physics schemes.

Table 2 shows the results of the 5-yr average meteorological variables from the 2001-2005 WRF_CCSM simulations. The model performance is overall similar to the base year of 2002

shown in Table 1. Compared to the performance of WRF-NCEP in 2002, WRF_CCSM simulations give larger overpredictions in WS10 in both winter and summer (due mainly to the use of meteorological fields from CCSM instead those from NCEP for nudging), and underpredictions in Precip. This reflects the limited capability of WRF_CCSM in capturing some meteorological variables at mesoscale and local scales, which could be partly related to biases in the CCSM BCs, in addition to the limitations of the above physics schemes in WRF. Overall, the meteorological predictions of WRF over the U.S. represent a good approximation of the seasonal climatology of the current atmosphere, with the performance generally consistent with or even better than that of previous MM5 and WRF applications (e.g., Dolwick et al., 2007; Zhang et al., 2010b, 2012).

3.2 Chemical predictions

Table 3 summarizes the domain-wide, seasonal statistical performance of CMAQ driven by WRF_NCEP initialization for surface concentrations, wet deposition fluxes, visibility parameters, and column abundances in winter and summer 2002. Predictions of maximum 1-h and 8-h O_3 compare well with observations, with NMBs and NMEs ranging from -11.1% to 11.4% and 15.5-28.6%, respectively, for the AIRS-AQS, CASTNET, and SEARCH sites in both seasons. Figure S1 in the supplementary material shows the spatial distribution of NMBs of maximum 8-h O_3 mixing ratios at all monitoring sites sites, with overpredictions at some AIR-AQS sites in both seasons and at the SEARCH sites during summer and underpredicted at the CASTNET sites in both seasons. Discrepancies between model predictions and observations in this work for O_3 may be due to uncertainties in the emissions of precursors (e.g., nitrogen oxides (NO_x = NO + NO_2) and volatile organic compounds (VOCs)) (Wang and Zhang, 2012), inaccuracies in meteorological variables such as overpredictions in WS10, underpredictions in T2, and inaccurate PBLH. As shown in Table 3, CO mixing ratios at the SEARCH sites are underpredicted. While this underprediction may be caused by several factors (e.g., an underestimate of CO emissions and an overestimate in dry deposition), one possible factor is an overestimate of simulated PBLH, which increases mixing

and leads to underpredictions of CO, NO, and HNO_3 at the SEARCH sites. In addition to the possible bias in PBLH, the underpredictions in NO_x emissions may be another reason for large underpredictions of NO and HNO_3 at the SEARCH sites. Finally, the grid resolution of 36-km is too coarse to capture meteorological phenomena and chemistry at fine- or meso- scales.

Table 3 also shows the performance of WRF_NCEP/CMAQ for $PM_{2.5}$ and its components (i.e., SO_4^{2-}, NO_3^-, NH_4^+, EC, and OC). Figure S1 shows the spatial distribution of NMBs of $PM_{2.5}$ over the U.S. in winter and summer. CMAQ generally overpredicts the concentrations of $PM_{2.5}$ and its components in winter while underpredicting them in summer. While the seasonal performance of those species at most sites is good to marginally good, large biases exist for some species at some sites. Discrepancies between observed and simulated $PM_{2.5}$ and its components may be due to a number of factors. These may include uncertainties in the emissions of gaseous precursors of secondary $PM_{2.5}$, as well as primary $PM_{2.5}$ (OC and EC), the model parameters such as the rate constant and heterogeneous reaction probability, and model representations of gas/particle partitioning, dry deposition, and scavenging/wet deposition fluxes (Wang and Zhang, 2012). The spatial variability and biases of meteorology and the use of a coarse grid resolution may also contribute to model biases in PM predictions. More detailed analyses of likely causes for such biases are provided in the supplementary material. The model evaluation results are generally consistent with those reported by other studies (Zhang et al., 2008, 2009a; Appel et al., 2011b; Wang and Zhang, 2012).

The performance statistics of WRF/CMAQ in capturing seasonal mean weekly total wet deposition fluxes of SO_4^{2-}, NO_3^-, and NH_4^+ is relatively good. Winter results show an underprediction of all fluxes (NMBs of -28.6% to -15.7%) while summer wet deposition flux is overpredicted for SO_4^{2-} and NH_4^+ (NMBs of 24.6% and 36.3%, respectively) but underpredicted for NO_3^- (an NMB of -21.6%). The underprediction of wet deposition fluxes in winter may be due to the underprediction in Precip in winter rather than the aqueous-phase concentrations of depositing

291 species, as their particulate concentrations are overpredicted (except for NO_3^- at the CSN and
292 SEARCH sites). The dependent relationship between wet deposition fluxes and Precip may also be
293 true for SO_4^{2-} and NH_4^+ in summer, in that an overprediction of Precip may cause the
294 overprediction of wet deposition fluxes of SO_4^{2-} and NH_4^+ despite an underprediction in their
295 particulate concentrations. In summer, one exception is NO_3^-, whose wet deposition fluxes are
296 underpredicted possibly due to the underprediction in its aqueous-phase concentrations as a result
297 of its underpredicted particulate concentrations (except at the SEARCH sites). Two visibility
298 parameters; β_{ext} and HI, based on the PM concentrations using the Mie theory are evaluated against
299 observations from IMPROVE. HI is well represented by CMAQ in winter with an NMB of 7% and
300 moderately underpredicted in summer with an NMB of -35.6%. CMAQ greatly overpredicts β_{ext} in
301 winter with an NMB of 89.2% but underpredicts it in summer with an NMB of -26.2%, consistent
302 with NMBs of $PM_{2.5}$ in both seasons.

303 The evaluation of simulated tropospheric column abundances of CO, NO_2, HCHO, TOR,
304 and AOD against observations is shown in Figure S2 and discussed in the supplementary material.
305 Overall, in terms of performance statistics, CMAQ predicts column CO and TOR fairly well, but
306 shows larger biases in predicted column HCHO and TOR, as well as AOD. CMAQ simulates
307 relatively well the spatial distributions for TOR and AOD in summer and CO and NO_2 in both
308 seasons but poor for HCHO in both seasons.

309 Table 4 shows the statistical performance of chemical predictions of the 5-year average of
310 WRF_CCSM simulations. Results are similar to the base year of 2002, indicating that
311 WRF_CCSM simulations of 2001-2005 represent current-year air quality.

312 **4. Change of future climate and emissions and their impacts on air quality**

313 **4.1 Future climate trends**

314 Figure 1 shows the differences of T2, RH2, GSW, and CFRAC, Precip, WS10, PBLH, and
315 the Monin-Obukhov Length (MOL) between the average of the future years (2026-2030) and the

316 average of the current years (2001-2005). These changes, which have strong influence on air
317 quality, are associated with changes in the thermodynamics of the atmosphere as well as dynamical
318 changes reflected in changes in synoptic circulation such as storm tracks and blocking high.
319 Warming occurs over nearly the entire U.S. in summer due to increases in greenhouse gases and
320 small increases in GSW, while warming on average of about 0.83 °C occurs for the eastern U.S. in
321 winter, with slight cooling over portions of the western U.S. Hogrefe et al. (2004) and Unger et al.
322 (2006) reported similar results with the largest increases in surface air temperature over the central
323 U.S. The changes in GSW and CFRAC follow each other inversely, especially in winter, where
324 decreases in GSW correspond to increases in CFRAC. Increased saturation of the air (RH2) in the
325 future increases CFRAC. Increases in CFRAC and decreases in GSW also lead to the decreases in
326 T2 over parts of the western U.S. Increased water vapor mixing ratio (not shown) in both summer
327 and winter results in increased RH2, with exceptions in summer over portions of the lower plains
328 and Texas. Areas with the largest increase in CFRAC, particularly the west coast and southeastern
329 U.S. in winter, experience the largest increase in Precip (up to 0.478 mm). Changes in Precip over
330 the U.S. in summer are relatively small and vary regionally. Winter WS10 decreases mainly in the
331 northern plains, southwestern U.S., and portions of the east coast, but increases over the rest of the
332 U.S., particularly over most of the western U.S. The general increase in WS10 over the western
333 U.S. is consistent with the increase in Precip over the region, suggesting an increased frequency of
334 Pacific storms, leading to increased Precip, PBLH, and WS10. Summer WS10 decreases over
335 much of the U.S., consistent with the overall reduced Precip and PBLH (by about 27.1 m)
336 corresponding to more stable atmospheric conditions.

337 Lam et al. (2011) reported a maximum increase of 184.2 m and a maximum decrease of
338 105.4 m in PBLH between May-September and a maximum increase of 117 m and a maximum
339 decrease of 93.1 m in PBLH during January-April by 2050. The variation in trend of PBLH in this
340 work is similar to that of Lam et al. (2011) in magnitude, with some spatial variability due to the

different seasons examined. MOL is used as a measure of atmospheric stability (Seinfeld and Pandis, 2006) with large (between 100 and 10^5 m) to small (< 100 m) positive values corresponding to stable and very stable conditions, respectively, and large (between -10^5 and -100 m) to small (> -100 m) negative values corresponding to unstable and very unstable conditions, respectively, and very large negative (< -10^5 m) or very large positive values (> 10^5 m) corresponding to neutral conditions. Current year winter conditions are very stable to stable over the western coastal area, the Southeast, and the lower central plains, while the Rocky Mountain region, the upper plains, the Great Lakes region, and the upper Northeast on average have a very unstable to unstable atmosphere (figures not shown). In the future, winter conditions in the southeast become less stable but may still remain in the stable regime, while over the west coast, conditions become less stable to very unstable, consistent with increased PBLH. Over the Rockies and other regions, conditions stay in the very unstable regime or change to stable (consistent with increased PBLH). For other regions, the conditions may remain very unstable or change to stable (consistent with reduced PBLH). Atmospheric stability in the summer becomes slightly more stable over most areas of the U.S., consistent with the decreased PBLH. Leung et al. (2005) reported a decrease in unvented hours (i.e., an increase in unvented hours is a negative impact on air quality) over the southeastern U.S. and Texas for JJA and September, October, November (SON), but reported increases over the central plains in JJA and western U.S. in SON. Zhang et al. (2008) predicted increases in MOL over the central, southeastern, and western coastal areas of the U.S. for future summer conditions. Spatially, Leung et al. (2005), Zhang et al. (2008), and this study differ in the predicted atmospheric stability. Uncertainties are also present in the simulated mixing depth among studies, with no clear regional agreement of increases or decreases (Hogrefe et al., 2004; Leung and Gustafson, 2005; S. Wu et al., 2008a; Chen et al., 2009; Jacob and Winner, 2009). This suggests that changes in atmospheric stability and mixing are highly uncertain because they are more strongly influenced by changes in large scale circulation that are less constrained than thermodynamical changes in

response to greenhouse warming. Tai et al. (2012) used historical data and showed that 20 – 40% of the observed $PM_{2.5}$ day-to-day variability is explained by cold frontal passages in the eastern U.S. and maritime inflow in the West, while interannual variability of $PM_{2.5}$ in the Midwest is correlated strongly with cyclone frequency. However, even among 5 ensemble members of the same GCM under the same emission scenario, the projected changes in cyclone frequency are inconsistent, suggesting large uncertainty in circulation changes that influence atmospheric stability and mixing and hence air quality.

4.2 Future anthropogenic and biogenic emissions

Projected decreases in anthropogenic emissions are expected to decrease chemical concentrations. Significant reductions in NO_x emissions (28%) are projected to decrease O_3 concentrations. The projected decreases in the emissions of SO_2, VOCs, primary $PM_{2.5}$ (i.e., elemental carbon, primary organic carbon, SO_4^{2-}, and other inorganic PM) (with growth factors of 0.25, 0.56-0.96, and 0.65-0.95, respectively, see Table S2) will decrease future $PM_{2.5}$ concentrations; however, increases in the concentrations of NH_3, HCHO, and NO_3^- (with growth factors of 1.34, 1.14, and 1.01, respectively) may increase $PM_{2.5}$ concentrations in some regions. While the decreases in emissions are mainly due to emission control policy, the increases in emissions are associated with enhanced activities of specific sectors. For example, the increases in the emissions of NH_3 are due to enhanced emissions from agricultural operations and biomass burning, and those in emissions of HCHO are due to enhanced emissions from anthropogenic sources and biomass burning projected for future years. While the increases in the emissions of NH_3 and NO_3^- can directly increase $PM_{2.5}$ concentrations, the increases in the emissions of HCHO increases the mixing ratios of HCHO in both winter and summers (figures not shown), which lead to increased levels of CO, OH, HO_2, and HNO_3 through its reactions. The increases in the concentrations of OH, HO_2, and HNO_3 can result in the increases in the concentrations of NO_3^- and SOA in some areas in both seasons as shown in Figure 2. As changes in $PM_{2.5}$ concentrations are

affected by changes in the emissions of primary $PM_{2.5}$ and gaseous precursors of secondary $PM_{2.5}$, the dry, wet, and total deposition fluxes of PM will also be directly affected.

Winter trends of isoprene and terpene are similar with the largest increases over the Southeast, especially Florida in the summer, and decreases over the western U.S. The magnitude of the changes depends on vegetation species and associated BVOCs, but the spatial distribution correlates well with temperature changes for both summer and winter. Decreases in temperature over the western U.S. in winter lead to decreases in isoprene and terpene emissions, while increases in temperatures over the Southeast increase isoprene and terpene emissions. Summer temperatures increase over nearly the entire domain, especially over the Midwest, resulting in increased BVOCs emissions over most of the domain. The increasing trend of BVOCs emissions found in this study are similar to other studies that predicted increases of BVOC emissions by 10-90% due to increases of temperatures by mid-century and 2100, but the magnitude of their increases found in this study is smaller compared to other studies (e.g., Hogrefe et al., 2004; Tagaris et al., 2007; Zhang et al., 2008). Differences among BVOCs emissions predicted in these studies may be due to differences in the simulation period, the biogenic emission model and version used, and the projected climate change of each study. For example, BEIS versions 3.13 and 3.12 are used in this work and Zhang et al. (2008), respectively. In BEIS version 3.13, BVOCs emission parameterizations that account for the effects of leaf temperature and solar radiation are revised based on more recent case studies, generating more accurate BVOCs emissions than BEIS version 3.12.

4.3 Impacts of changes in both climate and emissions on regional air quality

Figure 2 shows the influence of future climate and emission projections on selected air quality variables including the absolute change in maximum 1-h and 8-h average O_3 mixing ratios, 24-h $PM_{2.5}$ and its composition concentrations, HI, and β_{ext}. Both maximum 1-h and 8-h average O_3 mixing ratios decrease over most of the western U.S. and parts of the Southeast in winter by about 1.5-2.0 ppb, but increase by up to 5.0 ppb over the eastern and southeastern U.S. and major

cities across the U.S.. Decreases in O_3 mixing ratios in winter, particularly over the western U.S., are largely due to increased PBLH, WS10, and CFRAC and decreased GSW. Zhang et al. (2009b) performed a full-year regional study on O_3 and $PM_{2.5}$ in the U.S. and found that in winter, VOC-limited O_3 chemistry dominates most of the U.S. with the exception of some areas in the western U.S. This may explain the increased O_3 mixing ratios in winter over the eastern U.S. and major cities found in this study, as BVOC emissions are projected to increase in winter, while only one anthropogenic VOC is projected to increase (i.e., formaldehyde). Areas of O_3 mixing ratio increases in winter may also be due to increased T2 and decreased WS10.

Summer maximum 8-h average O_3 mixing ratios decrease over nearly the entire U.S. on average of about 1.4 ppb, with the exception of major cities (e.g., Los Angeles, Chicago, Houston, St. Louis, and New York City) and the upper Midwest and the northern Rockies where increases in O_3 mixing ratios occur. Decreases in summer O_3 mixing ratios in this study are largely due to decreases in NO_x emissions (by 28%) and the NO_x-limited O_3 chemistry in summer. Zhang et al. (2009b) reported that O_3 chemistry over most of the U.S. switches from VOC-limited to NO_x-limited by April through August, with the exception of many major cities where O_3 chemistry remains VOC-limited. These results of future O_3 trends are similar to previous studies that examined the impacts of both climate and anthropogenic emissions. For example, Tagaris et al. (2007) reported a mean summer maximum daily average 8-h O_3 decrease of 11-28% by 2050 over the U.S. due to climate and emission reductions with the A1B scenario and Lam et al. (2011) reported a 10% or 5 ppb decrease of the annual maximum daily average 8-h O_3 over the eastern U.S. Unger et al. (2006) reported an increase in annual O_3 mixing ratios over the U.S. by 2030 with the A1B scenario; however, they attributed the increase mainly to methane (CH_4) emissions, which is not explicitly treated in CMAQ (although CMAQ accounts for the effect of CH_4 implicitly by using a background concentration of 1.85 ppm for CH_4). Although the increases in T2 over the U.S. in the summer and the eastern U.S. in the winter and resultant increases in BVOCs emissions

441 over most of the domain should cause increases in O_3 mixing ratios, the relationship among air
442 quality, emissions, and climate is not always linear and largely affected by various atmospheric
443 processes such as transport, gas-phase chemistry, and dry deposition (Zhang et al., 2009b). In
444 addition, Racherla and Adams (2008) and S. Wu et al. (2008b) indicated that while annual isoprene
445 emissions were predicted to increase in the Southeast, O_3 decreased due to NO_x sequestration in
446 reactions with isoprene and ozonolysis of isoprene. Decreases in O_3 while T2 and BVOCs increase
447 may also be due to the fact that emission reductions of O_3 precursors compensate for the effect of
448 climate change on O_3 formation, as discussed in Section 4.4.

449 Decreases in $PM_{2.5}$ concentrations are the most extreme over the eastern and central U.S. in
450 summer, with small decreases in the same regions in the winter. Slight increases are found over
451 small areas in the Southwest in summer and over the Great Lakes in winter. Decreases in winter
452 $PM_{2.5}$ concentrations can be attributed to the increases in Precip over much of the U.S. (which leads
453 to increased scavenging of $PM_{2.5}$ and its precursors), and decreases in the emissions of gaseous
454 precursor (e.g., SO_2) and primary PM (e.g., EC, primary OM, and other inorganic $PM_{2.5}$).
455 Decreases in summer $PM_{2.5}$ concentrations are due mainly to decreases in the aforementioned
456 emissions. Reductions in $PM_{2.5}$ concentrations in this study are similar to those found by Tagaris et
457 al. (2007) and Lam et al. (2011), who reported around a 35% decrease in summer average
458 concentrations of $PM_{2.5}$ and a 40-50% decrease in annual average $PM_{2.5}$ concentrations,
459 respectively, by 2050 with the A1B scenario. Decreases in HI and β_{ext} over most of the domain in
460 winter and summer are due to decreases in $PM_{2.5}$, indicating an improved visibility in the future.

461 The largest reduction in SO_4^{2-}, NH_4^+, and NO_3^- concentrations occur in summer, up to 6.2,
462 2.3 and, 1.4 $\mu g\ m^{-3}$, respectively), while spatially, OM and SOA decrease more in terms of
463 magnitude over a larger area in winter than summer. Decreases in NH_4^+, NO_3^-, SO_4^{2-}, OM, and
464 SOA are due to decreases in the emissions of gaseous precursors (e.g., NO_x, SO_2, and VOCs) and

primary PM species (e.g., OC), increased Precip in winter, and increased T2 that does not favor the formation of volatile PM species (e.g., NO_3^-, NH_4^+, and SOA). Increases in SOA and OM over most of the U.S. in summer may be due to increases in BVOCs emissions in both seasons. Increases in NO_3^- over most of the U.S. in winter may be due to increased NH_3 emissions and decreased SO_2 emissions that lead to changes in aerosol acidity driven by changes in the amounts of cation and anion in the particulate phase. Bauer et al. (2007) and Pye et al. (2009) found similar results for NO_3^-, in which its concentration increased over the northeastern U.S. due to increased availability of NO_x and NH_3 to form NO_3^-. Although NO_x emissions are reduced in this study, the increased availability of NH_3 may be due to increased emissions of NH_3 and reduced SO_4^{2-} concentrations (and consequently the availability for SO_4^{2-} to be neutralized by NH_4^+), resulting from decreased SO_2 emissions. Modeling SOA accurately is difficult, as its precursors, formation pathways, chemical composition, and physical properties are not fully understood. As shown in Figure 3, SOA increases over a small portion of the Southeast in winter and a large portion of the U.S. in summer, which is due to increases in BVOCs emissions. The decrease in SOA in winter and some regions in the eastern U.S. in summer may be attributed to changes in climatic conditions, such as increased T2 that compensates for the increases in SOA due to increased BVOCs emissions, similar to the annual mean results of Tsigaridis and Kanakidou (2007) and the summer results of Zhang et al. (2008). Zhang et al. (2008) found that although BVOC emissions increased SOA formation, future (i.e., 2050) climatic conditions, specifically increased T2, decreased SOA concentrations over the U.S. in summer. Tsigaridis and Kanakidou (2007) simulated future SOA concentrations with a fixed temperature increase of 1-2°C, while holding all other climatic conditions constant, and predicted an 11% decrease in SOA burden. Similar to $PM_{2.5}$ concentrations, HI and β_{ext} will decrease in most of the domain in both seasons except for the northeastern portion in winter.

Figure 3 shows absolute changes in seasonal-mean dry, wet, and total deposition fluxes of NH_4^+, NO_3^-, and SO_4^{2-}. Deposition fluxes are influenced by emissions and climate change. For

example, dry deposition is inversely related to total resistances (i.e., the total of aerodynamic, quasi-laminar, and surface resistance), so as resistances increase, dry deposition fluxes decrease (Seinfeld and Pandis, 2006). Increases in dry deposition fluxes of NH_4^+ and NO_3^- in winter are due to increases in emissions (e.g., NH_3 and NO_3^-), increases in concentrations of NO_3^-, and decreases in stomatal resistance (figures not shown), dominating over the increases in aerodynamic resistance. Areas of increased NO_3^- levels in winter generally correlate with the NO_3^- dry deposition fluxes, while the very small increase in NH_4^+ dry deposition fluxes do not correlate with NH_4^+ concentrations, but may be due to increases in dry deposition velocity. Decreases in dry deposition flux of SO_4^{2-} in the Southeast and increases in the west coast may likely be dominated by the increases in aerodynamic resistance and decreases in surface resistance, respectively. The decreases in the dry deposition fluxes of NH_4^+ and SO_4^{2-} in the future summer are likely dominated by increases in aerodynamic resistance domainwide, while the increases in the NO_3^- dry deposition fluxes over the Northeast are due to the increases in NO_3^- concentrations and decreases in decreases in stomatal resistance over the northern portion of the domain. Wet deposition of species is dependent on changes in precipitation and ambient concentrations of species. Precip increases over most of the U.S. in winter lead to increases in wet deposition fluxes of NH_4^+ and NO_3^- (by up to 0.29 g ha^{-1} and 0.60 g ha^{-1}, respectively). Wet deposition fluxes of SO_4^{2-} increase in winter over the west coast due to increased Precip, but decrease over the eastern U.S. in winter and summer due to large decreases of ambient SO_4^{2-} concentrations and SO_2 emissions. Summer Precip is more spatially variable than winter, but correlates well with wet deposition fluxes of NH_4^+ and NO_3^- (e.g., increased Precip leads to increased deposition fluxes and vice versa). Wet deposition changes dominate changes in total deposition for all species in winter and summer.

4.4 Impacts of projected anthropogenic emission changes on regional air quality

Figure 4 shows the impact of projected anthropogenic emissions on maximum 8-h average O_3 and $PM_{2.5}$ concentrations during future winter and summer with potentially good and poor air

quality by comparing the baseline simulation with both climate change and emission change and the sensitivity simulations with emissions kept at the 2002 levels. The relative impact of projected anthropogenic emissions on the concentrations of O_3 and $PM_{2.5}$ is nearly the same for both poor and good air quality winters in 2026 and 2029, respectively. This is expected, as projected anthropogenic emissions are the same in winters 2026 and 2029. Because projected anthropogenic emissions of NO_x and all VOCs except for HCHO are lower, domainwide maximum 8-h average O_3 mixing ratios decrease by 0.08-0.1 ppb and 2.8-3.0 ppb for future winters and summers, respectively. However, maximum 8-h average O_3 mixing ratios in eastern U.S. increase by up to 4.1 and 5.0 ppb during a good air quality winter in 2029 and a poor air quality winter in 2026, respectively. This is because more OH radicals (as a result of lower SO_2 and NO_x emissions) become available for the oxidation of isoprene, leading to increased O_3 that dominates over decreases in O_3 resulted from reduced O_3 precursors in this region during winters. During future poor and good air quality winters, the domain-wide decreases and regional increases in O_3 levels are much smaller than those predicted from the averaged changes of O_3 levels in 5 winters during 2026-2030 changes shown in Figure 2, indicating a dominant role of climate changes in affecting future O_3 levels. During future poor and good air quality summers, the domain-wide decreases in O_3 levels are comparable to or even larger than the averaged changes of O_3 levels in 5 summers during 2026-2030 shown in Figure 3, indicating a more important role of anthropogenic emissions in affecting future O_3 levels. Because of projected reduced primary PM emissions such as SO_4^{2-}, OM, and other inorganic PM and emissions of secondary PM such as SO_2, NO_x, and VOCs, domain-wide $PM_{2.5}$ concentrations decrease by 0.6-0.7 and 1.4-1.6 $\mu g\ m^{-3}$, with larger decreases in eastern U.S. by up to 5.4-5.7 and 16.5-16.6 $\mu g\ m^{-3}$ for future winter and summer, respectively. These decreases are comparable to or even larger than those predicted from averaged changes of $PM_{2.5}$ concentrations in the 2026-2030 summers and winters shown in Figure 2, indicating that

539 significant reductions in anthropogenic emissions can dominate over the effects of climate change.
540 Despite the potentially dominant role of anthropogenic emission changes, climate change may have
541 a greater or dominant impact on several gaseous and PM species such as BVOCs, SOA, NH_4^+, and
542 NO_3^- (figures not shown), as compared to anthropogenic emission changes. As expected, reducing
543 anthropogenic emissions can reduce more $PM_{2.5}$ in summer than in winter. Further, reducing
544 precursor emissions under poor air quality winter (2026) and summer (2029) will lead to greater
545 reductions in $PM_{2.5}$ concentrations compared to good air quality winter (2029) and summer (2030).

546 Results shown in this work are similar to those of other studies that examined the separate
547 and/or combined impacts. Several studies (e.g., Hogrefe et al., 2004; Tagaris et al., 2007; S. Wu et
548 al., 2008b; Zhang et al., 2008; Lam et al., 2011) predicted increases in maximum 8-h average O_3
549 over the Midwest and eastern U.S. for future years (2020 or 2050) due to climate change alone,
550 with the exception of Tagaris et al. (2007) that predicted a slight (0.1%) increase in the Midwest
551 and Zhang et al. (2008) that predicted a slight decrease over the northern plains (about 1.0 ppb).
552 Weaver et al. (2009) conducted a study with seven regional air quality models, all predicting an
553 increase in 2050 summer O_3 concentrations due to climate change alone of about 2-8 ppb over the
554 U.S., with some regions showing little or slight decreases. Their study stated, however, that the
555 regional patterns of O_3 change did not always agree among simulations due to differences in
556 modeling systems, configurations, and the experiment design choices of each group/simulation.
557 Weaver et al. (2009) also pointed out that O_3 concentrations seem to correspond relatively well to
558 temperature and surface insolation in most of their simulations; however, some areas show no
559 correspondence to these two variables. Changes in O_3 concentration may be due to other forcing
560 factors such as Precip and wind speed, which could also be factors in this study as well. In general,
561 many previous studies have found that future anthropogenic emissions have a greater influence
562 compared to climate change alone on future air quality, specifically projected emission reductions
563 that reduce O_3 and/or $PM_{2.5}$ concentrations, which is also shown in this study.

5. Conclusions

In this study, WRF and the newly released CMAQ v5.0 are used to examine the impacts of changing climate and anthropogenic emission projections on future (2026-2030) air quality, as compared to current conditions (2001-2005) over the contiguous U.S. Current years (2002 for WRF_NCEP and 2001 – 2005 for WRF_CCSM) simulations of meteorological variables, chemical concentrations, wet deposition, visibility, and column mass abundance capture the overall observational spatial patterns and seasonal differences. WRF and CMAQ perform similarly in terms of performance statistics to other regional models reported in other studies. Large biases in some meteorological variables from WRF_NCEP and WRF_CCSM simulations (e.g., WS10 and Precip) are attributed to limitations in the PBL, land-surface, cumulus, and microphysics schemes as well as the limited capability of CCSM in capturing these variables at mesoscale and local scales. Biases in O_3 predictions may be due to uncertainties in the emissions of precursors and inaccuracies in some meteorological variables (e.g., overpredictions in WS10 and underpredictions in T2). Biases in predictions of $PM_{2.5}$ and its components can be attributed to uncertainties in the emissions of primary $PM_{2.5}$ and precursors of secondary $PM_{2.5}$, uncertainties in model representations of some atmospheric processes (e.g., gas/particle partitioning and scavenging/wet deposition), and inaccurate meteorological predictions. The use of a coarse horizontal grid resolution of 36-km contributes to model biases in meteorological and chemical predictions.

Future (2026-2030) winter climatic conditions are predicted to be colder with increased mixing (PBLH) in the west, but warmer with decreased mixing in the east, and with increased cloud cover, increased moisture and precipitation over the contiguous U.S. The summer, however, is predicted to be warmer with decreased PBLH over most of the U.S., but with other climatic conditions showing slight deviations from current conditions and spatial variability compared to winter. Increases in summer and winter temperatures are predicted to increase BVOCs emissions

589 over most of the domain, with the exception of California and the Pacific Northeast in winter.
590 Increases in future BVOCs emissions could potentially lead to increases in O_3 mixing ratios in
591 VOC-limited regions; however, projected anthropogenic emissions of O_3 precursors decrease,
592 which dominates over the effect of climate alone over most of the domain in summer and the
593 western U.S. in winter. Maximum 1-h and 8-h average O_3 mixing ratios are predicted to decrease
594 by as much as 12.6 ppb during summer conditions over much of the domain, whereas major cities
595 in both summer and winter and the east coast in the winter show an increase by as much as 9.1 ppb.
596 Winter and summer $PM_{2.5}$ concentrations are also affected by future climate and
597 anthropogenic emission projections. Decreases in $PM_{2.5}$ and its components are mainly due to the
598 decreases in gaseous precursors and primary PM emissions and increases in precipitation in winter.
599 Concentrations of $PM_{2.5}$ decrease by as much as 5.7 $\mu g\ m^{-3}$ in winter and 9.9 $\mu g\ m^{-3}$ in summer due
600 to decreases in the concentrations of $PM_{2.5}$ components, particularly OM, NH_4^+, and SO_4^{2-} in winter
601 and NH_4^+, NO_3^-, and SO_4^{2-} in summer. Increases in OM in summer can be attributed to increases in
602 SOA, which is in turn due to increases in BVOCs emissions. Future decreases in $PM_{2.5}$ levels also
603 lead to improved visibility. Dry deposition fluxes of NH_4^+ and NO_3^- increase in winter over much
604 of the U.S. due to increased ambient concentrations and decreased surface resistance, while their
605 wet deposition fluxes in winter increase due to increased Precip. Summer wet deposition of NH_4^+
606 and NO_3^- are more spatially variable than winter, with decreases corresponding to decreases in
607 precipitation and ambient concentration. SO_4^{2-} dry, wet, and total deposition fluxes decrease over
608 the eastern U.S. in summer and winter due to decreases in SO_4^{2-} concentrations.
609 Overall, air quality improves more in summer than winter. Winter concentrations of O_3,
610 $PM_{2.5}$, NH_4^+, and NO_3^- either decrease less or increase compared to summer concentrations,
611 especially over the eastern U.S. because of the larger increase in T2. Visibility (HI and β_{ext})
612 improves in both winter and summer, with the exception of the Great Lakes region and some areas

of the eastern U.S in winter. Spatially on average, the total deposition fluxes of aerosols decreases more in winter, while total deposition fluxes increases more in summer. Increased nitrogen deposition and acid rain can have negative influences on ecosystems, agriculture, and architecture. Seasonal differences in meteorological variables play a role in the variability between winter and summer air quality. For example, a larger increase in future T2 and a larger decrease in future PBLH over the east coast in winter lead to increases in O_3 mixing ratios in winter, whereas summer O_3 mixing ratios decrease due to smaller increases in T2 and decreased precursor emissions.

Sensitivity studies show that projected anthropogenic emission changes play a more important role in summer than in winter for future O_3 and $PM_{2.5}$ levels; and they dominate over climate changes for $PM_{2.5}$ during both summers and winters. While this study provides a comprehensive analysis on the impacts of future climate and emission projections on air quality, some limitations exist. This study did not account for changes in land use and land cover as well as vegetation although they may impact future air quality (S. Wu et al., 2012). The emissions of dust and lightning NO_x are not included, which would contribute to model biases. Their important roles have been recognized in a number of studies (e.g., Hudman et al., 2007; Wang et al., 2013). Other limitations include the uncertainties of emissions and emission growth factors, limited length of the simulations to establish more robust changes due to climate and emissions compared to interannual variability (due to computational constraints), use of a single GCM, regional model, and air quality model, and use of an offline-coupled WRF/CMAQ that does not consider the feedback of PM to climate. In particular, the use of uniform growth factors over the entire CONUS in this work will introduce some uncertainties in projection of future air quality due to different emission control strategies at different states. The accuracy of the projected emissions is critical to the reliability of the projected air quality because this study, as well as other previous studies, consistently show that overall the impacts of changes in anthropogenic emissions dominate the effects of climate change

on future air quality in the next few decades when the climate change signals in response to greenhouse warming are relatively weak.

Acknowledgments

This work was supported by National Research Initiative Competitive Grant no. 2008-35112-18758 from the USDA Cooperative State Research, Education, and Extension Service Air Quality Program and the Office of Science of the U.S. Department of Energy as part of the Regional and Global Climate Modeling Program. Thanks are owed to Dr. David Streets, Argonne National Laboratory, for providing the future anthropogenic emission growth factors; to the U.S. EPA for meteorological and chemical initial and boundary conditions and the 2002 emissions inventory; to Wei Wang, a visiting scholar at NCSU from the Institute of Atmospheric Physics, Chinese Academy of Science, and Wyat Appel and Robert Gilliam, U.S. EPA, for AMET support, and to Drs. Gary Howell and Eric Sills, NCSU, for computer system support. All satellite observations were downloaded from their receptive web sites.

The Pacific Northwest National Laboratory is operated for DOE by Battelle Memorial Institute under Contract DE-AC05-76RLO1830.

References

Alapaty, K., Herwehe, J. A., Otte, T. L., Nolte, C. G., Bullock, O. R., Mallard, M. S., Kain, J. S. and Dudhia, J., 2012. Introducing subgrid-scale cloud feedbacks to radiation for regional meteorological and climate modeling. Geophysical Research Letters 39, L24809, doi:10.1029/2012GL054031.

Appel, K. W., Gilliam, R. C., Davis, N., Zubrow, A., Howard, S. C., 2011a. Overview of the atmospheric model evaluation tool (AMET) v1.1 for evaluating meteorological and air quality models. Environmental Modelling & Software 26(4), 434-443, doi:10.1016/j.envsoft.2010.09.007.

661 Appel, K. W., Roselle, S. J., Pleim, J., Mathur, R., 2011b. Evaluation of CMAQ v5.0 Performance
662 for January and July 2006, 10th Annual CMAS Conference, Chapel Hill, NC.
663 Appel, K. W., Roselle, S. J., Gilliam, R. C., Pleim J. E., 2010. Sensitivity of the Community
664 Multiscale Air Quality (CMAQ) model v4.7 results for the eastern United States to MM5 and
665 WRF meteorological drivers. Geoscience Model Development 3, 169-188, doi:10.5194/gmd-3-
666 169-2010.
667 Appel, K.W., Pouliot, G. A., Simon, H., Sarwar, G., Pye, H. O. T., Napelenok, S. L., Akhtar, F.,
668 and Roselle, S. J., 2013. Evaluation of dust and trace metal estimates from the Community
669 Multiscale Air Quality (CMAQ) model version 5.0. Geoscience Model Development 6, 883-
670 899.

671 Bauer, S. E., Koch, D., Unger, N., Metzger, S. M., Shindell, D. T., Streets, D. G., 2007. Nitrate
672 aerosols today and in 2030: a global simulation including aerosols and tropospheric ozone.
673 Atmospheric Chemistry and Physics 7(19), 5043-5059.

674 Bey, I., Jacob, D., Yantosca, R., Logan, J., Field, B., Fiore, A., Li, Q., Liu, H., Mickley, L., and
675 Schultz, M., 2001. Global modeling of tropospheric chemistry with assimilated meteorology:
676 Model description and evaluation. Journal of Geophysical Research 106(D19), 23073-23095,
677 doi:10.1029/2001JD000807.

678 Brown, S. S., Stark, H., Ravishankara, A. R., 2003. Applicability of the steady state approximation
679 to the interpretation of atmospheric observations of NO_3 and N_2O_5. Journal of Geophysical
680 Research 108, 4539, doi:10.1029/2003JD003407.
681 Byun, D., Schere, K. L., 2006. Review of the governing equations, computational algorithms, and
682 other components of the models-3 Community Multiscale Air Quality (CMAQ) modeling
683 system. Applied Mechanics Reviews 59(1-6), 51-77, doi:10.1115/1.2128636.

684 Dawson, J. P., Racherla, P. N., Lynn, B. H., Adams, P. J., Pandis, S. N., 2009. Impacts of climate
685 change on regional and urban air quality in the eastern United States: Role of meteorology.
686 Journal of Geophysical Research 114(D05308), doi:10.1029/2008JD009849.

687 Dolwick, P., Gilliam, R., Reynolds, L., Huffman, A., 2007. Regional and Local-Scale Evaluation of
688 2002 MM5 Regional and Local-Scale Evaluation of 2002 MM5 Meteorological Fields for
689 Various Air Quality Modeling Applications, Presentation at the 6th Annual CMAS Conference,
690 Chapel Hill, 1-3 October.

691 Doherty, R. M., et al., 2013. Impacts of climate change on surface ozone and intercontinental ozone
692 pollution: A multi-model study. Journal of Geophysical Research 118, 3744–3763,
693 doi:10.1002/jgrd.50266.
694 Emmons, L. K., Edwards, D. P., Deeter, M. N., Gille, J. C., Campos, T., Nedelec, P., Novelli, P.,
695 Sachse, G., 2009. Measurements of Pollution In The Troposphere (MOPITT) validation through
696 2006. Atmospheric Chemistry and Physics 9(5), 1795-1803.

697 Fiore, A. M., Levy II, H., Jaffe, D. A., 2011. North American isoprene influence on
698 intercontinental ozone pollution. Atmospheric Chemistry and Physics 11, 1697–1710,
699 doi:10.5194/acp-11-1697-2011.

700 Gao, Y., Fu, J. S., Drake, J. B., Lamarque, J. F., Liu, Y., 2013. The impact of emission
701 and climate change on ozone in the United States under representative concentration
702 pathways (RCPs). Atmospheric Chemistry and Physics 13, 9607–9621, doi:10.5194/acp-13-
703 9607-2013.
704 Gilliam, R. C., Pleim, J. E., 2010. Performance assessment of new land surface and planetary
705 boundary layer physics in the WRF-ARW. Journal of Climate and Applied Meteorology 49,
706 760-774. doi: http://dx.doi.org/10.1175/2009JAMC2126.1.

707 Gilliam, R. C., Hogrefe, C., Rao, S.T., 2006. New methods for evaluating meteorological models
708 used in air quality applications. Atmospheric Environment 40, 5073-5086, doi:
709 10.1016/j.atmosenv.2006.01.023.
710 Guenther, A., Zimmerman, P., Harley, P., Monson, R., Fall, R., 1993. Isoprene and Monoterpene
711 Emission Rate Variability - Model Evaluations and Sensitivity Analyses. Journal of
712 Geophysical Research 98(D7), 12609-12617, doi:10.1029/93JD00527.

713 Hogrefe, C., Lynn, B., Civerolo, K., Ku, J., Rosenthal, J., Rosenzweig, C., Goldberg, R., Gaffin,
714 Knowlton, S., K., Kinney, P, 2004. Simulating changes in regional air pollution over the eastern
715 United States due to changes in global and regional climate and emissions. Journal of
716 Geophysical Research 109(D22), D22301, doi:10.1029/2004JD004690.

717 Hudman, R. C. et al., 2007. Surface and lightning sources of nitrogen oxides
718 over the United States: Magnitudes, chemical evolution, and outflow. Journal of Geophysical
719 Research 112, D12S05, doi:10.1029/2006JD007912.

720 IPCC, 2001. Climate Change 2001: The Scientific Basis-Contribution of Working Group I to the
721 Third Assessment Report of the Intergovernmental Panel on Climate Change. Cambridge
722 University Press, New York, 881 pp.
723 Jacob, D. J., Winner, D. A., 2009. Effect of climate change on air quality. Atmospheric
724 Environment 43(1), 51-63, doi:10.1016/j.atmosenv.2008.09.051.

725 Lam, Y. F., Fu, J. S., Wu, S., Mickley, L. J., 2011. Impacts of future climate change and effects of
726 biogenic emissions on surface ozone and particulate matter concentrations in the United States.
727 Atmospheric Chemistry and Physics 11(10), 4789-4806, doi:10.5194/acp-11-4789-2011.

728 Lei, H., Wuebbles, D. J., Liang, X.-Z., 2012. Projected risk of high ozone episodes in
729 2050. Atmospheric Environment, 59, 567–577, doi:10.1016/j.atmosenv.2012.05.051.

730 Leung, L., Gustafson, W., 2005. Potential regional climate change and implications to US air
731 quality. Geophysical Research Letters 32(16), L16711, doi:10.1029/2005GL022911.

732 Mass, C., Ovens, D., 2011. Fixing WRF's high speed wind bias: A new subgrid scale drag
733 parameterization and the role of detailed verification, Preprints, 24th Conference on Weather and
734 Forecasting/20th Conference on Numerical Weather Prediction, Seattle, W.A., American
735 Meteorological Society, 9B.6 (Available online at
736 http://ams.confex.com/ams/91Annual/webprogram/Paper180011.html).
737 Manders, A. M. M., van Meijgaard, E., Mues, A. C., Kranenburg, R., van Ulft, L. H.,
738 Schaap, M., 2012. The impact of differences in large-scale circulation output from climate models
739 on the regional modeling of ozone and PM. Atmospheric Chemistry and Physics 12, 9441-9458.
740 Nolte, C. G., Gilliland, A. B., Hogrefe, C., Mickley, L. J., 2008. Linking global to
741 regional models to assess future climate impacts on surface ozone levels in the
742 United States. Journal of Geophysical Research 113, D14307, doi:10.1029/2007JD008497.

743 Pye, H. O. T., Liao, H., Wu, S., Mickley, L. J., Jacob, D. J., Henze, D. K., Seinfeld, J. H., 2009.
744 Effect of changes in climate and emissions on future sulfate-nitrate-ammonium aerosol levels in
745 the United States. Journal of Geophysical Research 114, D01205, doi:10.1029/2008JD010701.

746 Racherla, P. N., Adams, P. J., 2008. The response of surface ozone to climate change over the
747 Eastern United States. Atmospheric Chemistry and Physics 8(4), 871-885.

748 Seigneur, C., Pun, B., Pai, P., Louis, J., Solomon, P., Emery, C., Morris, R., Zahniser, M.,
749 Worsnop, D., Koutrakis, P., White, W., Tombach, I., 2000. Guidance for the performance
750 evaluation of three-dimensional air quality modeling systems for particulate matter and
751 visibility. Journal of the Air & Waste Management Association 50(4), 588-599.

752 Seinfeld, J.H., Pandis, S. N., 2006. Atmospheric Chemistry and Physics: From Air Pollution to
753 Climate Change. John Wiley, Hoboken N.J., pp. 1203.
754 Skamarock, W.C., Klemp, J. B., Dudhia, J., Gill, D. O., Barker, D. M., Duda, M. G., Huang, X.-Y.,
755 Wang, W., Powers, J. G., 2008. A Description of the Advanced Research WRF Version 3.
756 NCAR Tech Note NCAR/TN 475 STR, pp.125 (Available from: UCAR Communications, P.O.
757 Box 3000, Boulder, CO 80307).
758 Stevenson, D. S., Young, P. J., Naik, V., Lamarque, J. F., Shindell, D. T., Voulgarakis, A.,
759 Skeie, R. B., Dalsoren, S. B., Myhre, G., Berntsen, T. K., Folberth, G. A., Rumbold, S. T.,
760 Collins, W. J., MacKenzie, I. A., Doherty, R. M., Zeng, G., van Noije, T. P. C., Strunk, A.,
761 Bergmann, D., Cameron-Smith, P., Plummer, D. A., Strode, S. A., Horowitz, L., Lee, Y. H.,
762 Szopa, S., Sudo, K., Nagashima, T., Josse, B., Cionni, I., Righi, M., Eyring, V., Conley, A.,
763 Bowman, K. W., Wild, O., 2012. Tropospheric ozone changes, radiative forcing and attribution
764 to emissions in the Atmospheric Chemistry and Climate Model Inter-comparison Project
765 (ACCMIP). Atmospheric Chemistry and Physics 13, 3063–3085.
766 Stauffer, D., Seaman, N., Binkowski, F., 1991. Use of four-dimensional data assimilation in a
767 limited-area mesoscale model Part II: Effects of data assimilation within the planetary
768 boundary layer. Monthly Weather Review 119, 734-754.
769 Tagaris, E., Manomaiphiboon, K., Liao, K., Leung, L. R., Woo, J., He, S., Amar, P., Russell, A. G.,
770 2007. Impacts of global climate change and emissions on regional ozone and fine particulate
771 matter concentrations over the United States. Journal of Geophysical Research 112(D14),
772 D14312, doi:10.1029/2006JD008262.

773 Tai, A. P. K., Mickley, L. J., Jacob, D. J., 2012. Impact of 2000–2050 climate change
774 on fine particulate matter ($PM_{2.5}$) air quality inferred from a multi-model analysis of
775 meteorological modes. Atmospheric Chemistry and Physics 12, 11329–11337, doi:10.5194/acp-
776 12-11329-2012.
777 Tsigaridis, K., Kanakidou, M., 2007. Secondary organic aerosol importance in the future
778 atmosphere. Atmospheric Environment 41(22), 4682-4692,
779 doi:10.1016/j.atmosenv.2007.03.045.

Unger, N., Shindell, D. T., Koch, D. M., Amann, M., Cofala, J., Streets, D. G., 2006. Influences of man-made emissions and climate changes on tropospheric ozone, methane, and sulfate at 2030 from a broad range of possible futures. Journal of Geophysical Research 111(D12), D12313, doi:10.1029/2005JD006518.

Wang, K., Zhang, Y., 2012. Application Evaluation, and Process Analysis of the US EPA's 2002 Multiple-Pollutant Air Quality Modeling Platform. Atmos. Clim. Sci., 2, 254-289, doi:10.4236/acs.2012.23025.

Wang, K., Zhang, Y., Nenes, A., Fountoukis, C., 2012. Implementation of Dust Emission and Chemistry into the Community Multiscale Air Quality Modeling System and Initial Application to An Asian Dust Storm Episode. Atmospheric Chemistry and Physics, 12, 10209–10237, doi:10.5194/acp-12-10209-2012.

Weaver, C. P., Cooter, E., Gilliam, R., Gilliland, A., Grambsch, A., Grano, D., Hemming, B., Hunt, S. W., Nolte, C., Winner, D. A., Liang, X.-Z., Zhu, J., Caughey, M., Kunkel, K., Lin, J. -T., Tao, Z., Williams, A., Wuebbles, D. J., Adams, P. J., Dawson, J. P., Amar, P., He, S., Avise, J., Chen, J., Cohen, R. C., Goldstein, A. H., Harley, R. A., Steiner, A. L., Tonse, S., Guenther, A., Lamarque, J. -F., Wiedinmyer, C., Gustafson, W. I, Leung, L. R., Hogrefe, C., Huang, H.-C., Jacob, D. J., Mickley, L. J., Wu, S., Kinney, P. L., Lamb, B., Larkin, N. K., McKenzie, D., Liao, K. -J., Manomaiphiboon, K., Russell, A. G., Tagaris, E., Lynn, B. H., Mass, C., Salathé, E., O'Neill, S. M., Pandis, S. N., Racherla, P. N., Rosenzweig, C, Woo, J. -H., 2009. A Preliminary Synthesis of Modeled Climate Change Impacts on US Regional Ozone Concentrations. Bulletin of the American Meteorological Society 90(12), 1843-1863, doi:10.1175/2009BAMS2568.1.

Wu, S., Mickley, L. J., Kaplan, J. O., Jacob, D. J., 2012. Impacts of changes in land use and land cover on atmospheric chemistry and air quality over the 21st century. Atmospheric Chemistry and Physics 12(3), 1597-1609, doi:10.5194/acp-12-1597-2012.

Wu, S., Mickley, L. J., Leibensperger, E. M., Jacob, D. J., Rind, D., Streets, D. G., 2008a. Effects of 2000-2050 global change on ozone air quality in the United States. Journal of Geophysical Research 113(D6), D06302, doi:10.1029/2007JD008917.

Wu, S., Mickley, L. J., Jacob, D. J., Rind, D., Streets, D. G., 2008b. Effects of 2000-2050 changes in climate and emissions on global tropospheric ozone and the policy-relevant background

surface ozone in the United States. Journal of Geophysical Research 113(D18), D18312, doi:10.1029/2007JD009639.

Young, P. J., Archibald, A. T., Bowman, K. W., Lamarque, J. F., Naik, V., Stevenson, D. S., Tilmes, S., Voulgarakis, A., Wild, O., Bergmann, D., Cameron-Smith, P., Cionni, I., Collins, W. J., Dalsoren, S. B., Doherty, R. M., Eyring, V., Faluvegi, G., Horowitz, L. W., Josse, B., Lee, Y. H., MacKenzie, I. A., Nagashima, T., Plummer, D. A., Righi, M., Rumbold, S. T., Skeie, R. B., Shindell, D. T., Strode, S. A., Sudo, K., Szopa, S., Zeng, G., 2012. Pre-industrial to end 21st century projections of tropospheric ozone from the Atmospheric Chemistry and Climate Model Intercomparison Project (ACCMIP). Atmospheric Chemistry and Physics 13, 2063–2090.

Zhang, Y.-S., Chen, Y., Sarwar, G., Schere, K., 2012. Impact of gas-phase mechanisms on Weather Research Forecasting Model with Chemistry (WRF/Chem) predictions: Mechanism implementation and comparative evaluation. Journal of Geophysical Research 117, D01301, doi:10.1029/2011JD015775.

Zhang, Y., Dulière, V., Mote, P. W., Salathé Jr., E. P., 2009. Evaluation of WRF and HadRM Mesoscale Climate Simulations over the U.S. Pacific Northwest. Journal of Climate 22, 5511-5526, doi: 10.1175/2009JCLI2875.1.

Zhang, Y., Hu, X., Leung, L. R., W. I. Gustafson Jr., 2008. Impacts of regional climate change on biogenic emissions and air quality. Journal of Geophysical Research 113(D18), D18310, doi:10.1029/2008JD009965.

Zhang, Y., Liu, P., Pun, B., Seigneur, C., 2006. A comprehensive performance evaluation of MM5-CMAQ for the Summer 1999 Southern Oxidants Study episode - Part I: Evaluation protocols, databases, and meteorological predictions. Atmospheric Environment 40(26), 4825-4838, doi:10.1016/j.atmosenv.2005.12.043.

Zhang, Y., Vijayaraghavan, K., Wen, X., Snell, H. E., Jacobson, M. Z., 2009a. Probing into regional ozone and particulate matter pollution in the United States: 1. A 1 year CMAQ simulation and evaluation using surface and satellite data. Journal of Geophysical Research 114, D22304, doi:10.1029/2009JD011898.

Zhang, Y., Wen, X., Wang, K., Vijayaraghavan, K., Jacobson, M. Z., 2009b. Probing into regional O_3 and particulate matter pollution in the United States: 2. An examination of formation

mechanisms through a process analysis technique and sensitivity study. Journal of Geophysical Research 114, D22305, doi:10.1029/2009JD011900.

Zhang, Y., Liu, X.-H., Olsen, K., Wang, W.-X., Do, B., Bridgers, G., 2010a. Responses of future air quality to emission controls over North Carolina, Part II: Analyses of future-year predictions and their policy implications. Atmospheric Environment 44(23), 2767-2779.

Zhang, Y., Wen, X., Jang, C. J., 2010b. Simulating chemistry-aerosol-cloud-radiation-climate feedbacks over the continental US using the online-coupled Weather Research Forecasting Model with chemistry (WRF/Chem). Atmospheric Environment 44(29), 3568-3582, doi:10.1016/j.atmosenv.2010.05.056.

Zhang, Y., Olsen, K., Wang, K., 2013. Fine Scale Modeling of Agricultural Air Quality over the Southeastern United States using Two Air Quality Models, Part I. Application and Evaluation. Aerosol and Air Quality Research, 13 (4): 1231–1252.

Table 1
Seasonal statistical model evaluation of WRF_NCEP for winter and summer 2002

		Winter						Summer					
Variable	Database	No. of Data	Mean Obs	Mean Sim	NMB (%)	NME (%)	Corr	No. of Data	Mean Obs	Mean Sim	NMB (%)	NME (%)	Corr
T2 (°C)	CASTNET	94209	7.3	6.2	-15.1	34.0	0.86	174869	21.5	22.3	4.2	11.9	0.87
	SEARCH	16881	11.0	10.1	-7.6	25.2	0.87	15554	27.2	26.7	-2.0	9.4	0.72
	CSN	1884	8.1	6.5	-18.7	29.9	0.85	3345	25.0	24.4	-2.4	7.4	0.83
RH2 (%)	CASTNET	161484	68.1	81.1	19.1	24.1	0.64	173513	64.5	67.0	4.0	19.6	0.75
	SEARCH	16947	72.7	80.9	11.3	18.7	0.66	15187	76.6	75.6	-1.3	14.9	0.67
WS10 ($m\ s^{-1}$)	CASTNET	158190	2.7	4.0	50.3	71.2	0.50	171181	2.03	3.02	48.8	71.9	0.49
	SEARCH	15632	2.4	2.9	21.6	50.2	0.46	14833	1.8	2.2	23.1	51.1	0.48
Precip (mm)	NADP	2489	14.5	9.7	-33.2	52.0	0.83	2808	16.7	27.7	65.9	111.2	0.57

Table 2
Seasonal statistical model evaluation of WRF_CCSM for winter and summer of the current five-year mean (2001-2005)

		Winter						Summer					
Variable	Database	No. of Data	Mean Obs	Mean Sim	NMB (%)	NME (%)	Corr	No. of Data	Mean Obs	Mean Sim	NMB (%)	NME (%)	Corr
T2 (°C)	CASTNET	365092	6.8	5.9	-13.2	79.7	0.43	850779	20.9	21.2	1.7	21.0	0.65
	SEARCH	82928	9.3	10.6	-13.9	68.5	0.24	79765	26.1	25.7	-1.4	13.2	0.60
	CSN	9307	7.8	7.0	-10.6	67.4	0.42	15375	24.5	23.2	-5.6	14.3	0.47
RH2 (%)	CASTNET	701319	69.8	74.8	7.2	25.2	0.31	843305	67.3	64.6	-4.0	23.2	0.65
	SEARCH	83741	73.6	76.9	4.6	25.0	0.23	79427	80.1	76.9	-4.0	16.9	0.57
WS10 ($m\ s^{-1}$)	CASTNET	699011	2.6	5.3	104.2	126.3	0.13	835040	2.0	3.8	92.4	117.0	0.17
	SEARCH	79715	2.5	3.7	47.1	80.9	-0.01	77844	1.8	3.1	74.5	95.2	0.07
Precip (mm)	NADP	12689	15.1	12.1	-20.0	111.8	0.17	14561	19.3	2.2	-88.4	97.5	0.01

Table 3
Statistical performance of CMAQ surface concentrations for winter and summer of 2002 with WRF_NCEP initialization

		Winter						Summer					
Variable	Database	No. of Data	Mean Obs	Mean Sim	NMB (%)	NME (%)	Corr	No. of Data	Mean Obs	Mean Sim	NMB (%)	NME (%)	Corr
Max 1-h O_3 (ppb)	AIRS-AQS	14857	31.7	35.3	11.4	23.6	0.58	98889	62.7	65.0	3.7	18.5	0.71
	CASTNET	2217	33.3	30.0	-10.0	21.0	0.60	7149	61.5	54.7	-11.1	28.6	0.39
	SEARCH	716	37.6	38.9	3.4	18.0	0.69	652	62.8	60.2	-4.0	15.5	0.78
Max 8-h O_3 (ppb)	AIRS-AQS	14726	27.0	31.3	16.0	28.5	0.58	97322	55.4	60.7	9.6	19.8	0.72
	CASTNET	2176	30.0	29.0	-3.4	20.9	0.65	7046	55.4	54.7	-1.4	16.3	0.78
	SEARCH	713	31.4	34.7	10.5	22.4	0.71	636	52.0	56.6	8.7	17.6	0.81
Hourly avg. CO (ppb)	SEARCH	13791	308.2	271.3	-12.0	42.7	0.51	15711	248.7	187.5	-24.6	38.9	0.55
Hourly avg. NO (ppb)	SEARCH	14290	9.8	1.9	-80.9	90.1	0.3	15472	3.2	0.4	-87.1	90.7	0.36
Hourly avg. SO_2 (ppb)	SEARCH	14160	3.4	5.3	56.0	105.2	0.37	15604	2.0	2.5	26.3	116.3	0.23
24-h avg. SO_2 (μg m^{-3}) [a]	CASTNET	834	4.8	10.8	124.6	125.1	0.88	961	2.4	3.9	61.8	88.5	0.3
Hourly avg. HNO_3 (ppb)	SEARCH	11109	5.5	0.9	-83.2	92.2	0.06	8175	6.5	0.9	-86.4	91.2	0.21
24-h avg. HNO_3 (μg m^{-3}) [a]	CASTNET	833	1.2	1.7	50.8	61.8	0.72	961	2.3	2.2	-5.7	47.0	0.07
Hourly avg. NH_3 (ppb)	NCDENR	5418	4.8	2.5	-48.9	87.8	0.11	4771	14.9	10.5	-29.5	79.7	0.15
24-h avg. $PM_{2.5}$ (μg m^{-3})	IMPROVE	3505	3.8	5.71	51.2	78.9	0.71	3971	8.6	5.0	-42.1	52.6	0.46
	CSN	2254	12.7	15.6	23.1	58.4	0.38	3339	15.1	10.2	-32.8	39.2	0.69
Hourly avg. $PM_{2.5}$ (μg m^{-3})	SEARCH	10172	10.3	13.9	34.4	74.8	0.36	7314	14.7	9.1	-38.0	49.2	0.51
	NCDENR	6082	11.3	14.8	30.6	56.9	0.39	9848	18.5	8.6	-53.2	55.8	0.58
24-h avg. SO_4^{2-} (μg m^{-3}) [a]	CASTNET	835	1.7	2.5	44.3	54.9	0.73	961	4.8	3.4	-29.3	31.2	0.53
24-h avg. SO_4^{2-} (μg m^{-3})	IMPROVE	3527	0.92	1.3	44.8	68.6	0.75	4070	2.4	1.8	-24.5	37.4	0.89
24-h avg. SO_4^{2-} (μg m^{-3})	CSN	2233	2.3	3.1	36.4	62.9	0.6	3282	4.8	3.8	-21.3	33.7	0.85
Hourly avg. SO_4^{2-} (μg m^{-3})	SEARCH	4600	1.4	3.6	152.9	169.3	0.37	6358	1.6	4.3	165.5	173.6	0.57
24-h avg. NO_3^- (μg m^{-3}) [a]	CASTNET	834	1.4	1.8	25.3	71.1	0.65	961	0.5	0.4	-33.9	99.6	0.04
24-h avg. NO_3^- (μg m^{-3})	IMPROVE	3395	0.7	0.97	34.7	104.9	0.52	4060	0.3	0.2	-46.4	96.4	0.3
24-h avg. NO_3^- (μg m^{-3})	CSN	1980	3.1	2.9	-6.8	73.3	0.27	1907	1.1	0.8	-27.9	80.0	0.3
Hourly avg. NO_3^- (μg m^{-3})	SEARCH	7851	8.7	1.8	-79.2	82.6	0.14	7453	7.5	14.8	98.0	98.0	0.23
24-h avg. NH_4^+ (μg m^{-3}) [a]	CASTNET	834	0.9	1.1	30.5	43.7	0.81	961	1.5	1.1	-26.5	31.3	0.31
24-h avg. NH_4^+ (μg m^{-3})	IMPROVE	79	0.8	1.3	59.0	68.0	0.49	78	1.9	1.7	-11.9	37.1	0.65
24-h avg. NH_4^+ (μg m^{-3})	CSN	2234	1.4	1.6	17.9	62.0	0.4	3282	1.6	1.3	-18.6	38.8	0.76
Hourly avg. NH_4^+ (μg m^{-3})	SEARCH	5516	1.4	1.7	24.2	88.8	0.06	6349	0.5	1.3	199	227.5	0.32
24-h avg. EC (μg m^{-3})	IMPROVE	3487	0.23	0.233	1.3	56.5	0.63	3971	0.31	0.25	-18.6	64.6	0.49
	CSN	2215	0.75	0.85	13.2	62.9	0.38	3264	0.58	0.59	1.2	53.6	0.4
24-h avg. OC (μg m^{-3})	IMPROVE	3502	0.84	0.74	-11.2	58.6	0.58	3982	2.2	0.9	-60.1	75.8	0.47
24-h avg. TC (μg m^{-3})	IMPROVE	3512	1.1	0.97	-8.5	56.2	0.62	3985	2.5	1.1	-54.9	72.8	0.48
	CSN	2144	4.2	2.8	-32.7	51.7	0.37	3231	4.5	1.6	-65.6	67.8	0.34
Weekly total SO_4^{2-} (g ha^{-1})	NADP	1703	162	135	-15.7	61.1	0.67	1740	335	417	24.6	83.1	0.45
Weekly total NO_3^- (g ha^{-1})	NADP	1703	162	123	-24.4	57.9	0.52	1740	302	236	-21.6	61.8	0.38
Weekly total NH_4^+ (g ha^{-1})	NADP	1703	29	21	-28.6	62.6	0.5	1740	83	113	36.3	93.2	0.39
β_{ext} (m m^{-1})	IMPROVE	3454	28.5	53.9	89.2	104.7	0.69	3520	50.1	37.0	-26.2	40.7	0.74
HI (deciview)	IMPROVE	3454	11.1	11.9	7.0	33.2	0.79	3520	15.5	10.0	-35.6	37.3	0.82
Tropo. CO column[b]	MOPITT	16576	1.9	1.8	-8.1	10.9	0.64	16576	1.84	1.5	-17.0	19.0	0.46
Tropo. NO_2 column[a]	GOME	15414	2.1	3.0	43.4	68.8	0.78	16575	1.4	1.6	13.9	45.6	0.74
Tropo. HCHO column[a]	GOME	14606	3.6	2.7	-26.5	48.5	0.30	16576	4.7	7.1	52.0	68.5	0.32
Tropo. O_3 column[a]	TOMS/ SBUV	13710	28.4	31.6	11.3	13.5	0.27	13710	41.8	34.9	-16.8	18.0	0.71
Aerosol optical depth[a]	MODIS	13785	0.11	0.06	-41.8	56.8	-0.18	16576	0.21	0.13	-37.0	41.3	0.54

[a] CASTNET data are collected every week but reported as 24-hr average. [b] The units are $\times 10^{18}$ molecules cm^{-2} for CO column, $\times 10^{16}$ molecules cm^{-2} for NO_2 and HCHO column, and Dobson unit (DU) for O_3 column. N/A - not applicable (observations not available).

Table 4

Statistical performance of CMAQ surface concentrations for winter and summer of the current five-year mean (2001-2005) with WRF_CCSM initialization

		Winter						Summer					
Variable	Database	No. of Data	Mean Obs	Mean Sim	NMB (%)	NME (%)	Corr	No. of Data	Mean Obs	Mean Sim	NMB (%)	NME (%)	Corr
Max 1-h O_3 (ppb)	AIRS-AQS	49659	32.6	37.7	14.9	27.0	0.34	477124	58.6	68.1	16.1	37.2	0.24
	CASTNET	9552	34.1	31.5	-7.5	23.9	0.37	28414	57.5	56.6	-1.5	30.5	0.32
	SEARCH	2356	36.0	37.5	4.4	27.0	0.35	1646	58.3	56.6	-2.9	34.0	0.29
Max 8-h O_3 (ppb)	AIRS-AQS	49179	27.8	34.6	24.4	35.4	0.31	470300	51.6	61.1	19.0	37.9	0.25
	CASTNET	9370	30.8	31.2	1.2	25.2	0.39	27982	51.7	55.7	7.7	31.3	0.33
	SEARCH	2328	30.3	35.5	17.0	33.0	0.39	1609	49.1	53.4	8.7	36.0	0.33
Hourly avg. CO (ppb)	SEARCH	35772	336	229	-31.9	50.4	0.28	29963	237	184	-22.6	48.0	0.39
Hourly avg. NO (ppb)	SEARCH	36394	11.5	1.0	-90.9	94.9	0.12	30165	3.2	0.6	-82.3	91.4	0.26
Hourly avg. SO_2 (ppb)	SEARCH	35705	4.1	4.6	12.0	100.0	0.13	29847	2.0	2.6	30.2	125.2	0.16
24-h avg. SO_2 ($\mu g\ m^{-3}$)	CASTNET	4333	5.8	8.9	53.8	72.2	0.74	4792	2.3	5.5	142.4	171.1	0.13
Hourly avg. HNO_3 (ppb)	SEARCH	30037	6.0	0.8	-86.8	95.7	0.03	22205	3.7	0.9	-75.1	92.7	0.07
24-h avg. HNO_3 ($\mu g\ m^{-3}$)	CASTNET	4332	1.2	1.5	22.3	60.0	0.52	4792	1.9	2.4	27.2	74.1	0.05
24-h avg. $PM_{2.5}$ ($\mu g\ m^{-3}$)	IMPROVE	16063	3.9	4.1	4.0	74.0	0.43	15873	7.9	6.5	-17.6	66.1	0.25
	CSN	10803	13.0	10.0	-23.3	61.9	-0.05	15464	14.5	11.8	-19.1	56.1	0.24
Hourly avg. $PM_{2.5}$ ($\mu g\ m^{-3}$)	SEARCH	14004	11.4	10.9	-4.9	68.3	0.09	36849	33.5	41.3	23.4	32.4	0.49
24-h avg. SO_4^{2-} ($\mu g\ m^{-3}$) [a]	CASTNET	4333	1.9	1.6	-14.3	46.5	0.52	4792	4.6	4.1	-11.9	44.2	0.24
24-h avg. SO_4^{2-} ($\mu g\ m^{-3}$)	IMPROVE	16307	0.97	1.03	6.4	76.1	0.43	16185	2.4	2.3	-4.0	69.5	0.50
24-h avg. SO_4^{2-} ($\mu g\ m^{-3}$)	CSN	10669	2.4	1.9	-21.2	65.4	0.16	15436	4.8	4.4	-9.1	70.1	0.31
Hourly avg. SO_4^{2-} ($\mu g\ m^{-3}$)	SEARCH	6743	1.3	2.7	111.4	152.3	-0.03	11293	3.0	5.0	68.4	131.3	0.05
24-h avg. NO_3^- ($\mu g\ m^{-3}$) [a]	CASTNET	4333	1.6	1.4	-8.6	7.1	0.49	4792	0.53	0.42	-21.0	110.4	0.00
24-h avg. NO_3^- ($\mu g\ m^{-3}$)	IMPROVE	16145	0.82	0.64	-22.1	100.5	0.27	16167	0.28	0.16	-40.3	100.6	0.16
24-h avg. NO_3^- ($\mu g\ m^{-3}$)	CSN	9507	3.2	1.9	-39.4	80.6	0.00	13422	0.9	0.6	-30.6	95.0	0.05
Hourly avg. NO_3^- ($\mu g\ m^{-3}$)	SEARCH	10872	9.0	1.3	-85.8	89.2	0.05	12571	11.8	0.2	-98.1	98.4	0.10
24-h avg. NH_4^+ ($\mu g\ m^{-3}$) [a]	CASTNET	4333	0.9	0.9	-9.9	45.1	0.60	4791	1.5	1.4	-7.1	48.7	0.10
24-h avg. NH_4^+ ($\mu g\ m^{-3}$)	IMPROVE	1027	0.82	0.95	15.1	67.1	0.16	889	1.5	1.9	25.5	69.8	0.37
24-h avg. NH_4^+ ($\mu g\ m^{-3}$)	CSN	10663	1.6	1.1	-32.1	67.4	0.11	15423	1.6	1.5	-7.0	77.1	0.27
Hourly avg. NH_4^+ ($\mu g\ m^{-3}$)	SEARCH	8566	1.4	1.2	-13.4	82.6	0.00	11115	0.81	1.7	103.9	168.4	0.06
24-h avg. EC ($\mu g\ m^{-3}$)	IMPROVE	15968	0.22	0.16	-28.4	68.4	0.45	15882	0.29	0.29	0.8	76.8	0.14
	CSN	10580	0.7	0.5	-27.7	0.71	0.08	15335	0.55	0.65	17.3	66.6	0.24
24-h avg. OC ($\mu g\ m^{-3}$)	IMPROVE	16046	0.9	0.5	-42.9	73.9	0.31	15973	1.8	1.0	-42.5	86.4	0.07
24-h avg. TC ($\mu g\ m^{-3}$)	IMPROVE	16105	1.1	0.7	-40.0	71.8	0.36	15995	2.1	1.3	-36.4	82.8	0.08
	CSN	9647	4.0	1.7	-56.0	72.0	0.03	14688	3.8	1.9	-50.4	61.3	0.11
Weekly total SO_4^{2-} ($g\ ha^{-1}$)	NADP	7420	159	113	-29.2	96.8	0.11	7341	400	148	-62.9	86.1	0.14
Weekly total NO_3^- ($g\ ha^{-1}$)	NADP	7420	159	101	-36.7	84.8	0.15	7341	293	78	-73.4	86.1	0.07
Weekly total NH_4^+ ($g\ ha^{-1}$)	NADP	7420	27.5	18.6	-32.3	91.3	0.11	7298	79.6	33.9	-57.3	86.9	0.05
β_{ext} ($m\ m^{-1}$)	IMPROVE	15501	29.5	35.1	18.8	77.5	0.37	15038	46.5	43.9	-5.7	60.4	0.45
HI (deciview)	IMPROVE	15501	11.4	9.0	-21.1	46.1	0.54	15501	29.5	35.1	18.8	77.5	0.37

[a] CASTNET data are collected every week but reported as 24-hr average. N/A, not applicable (observations not available).

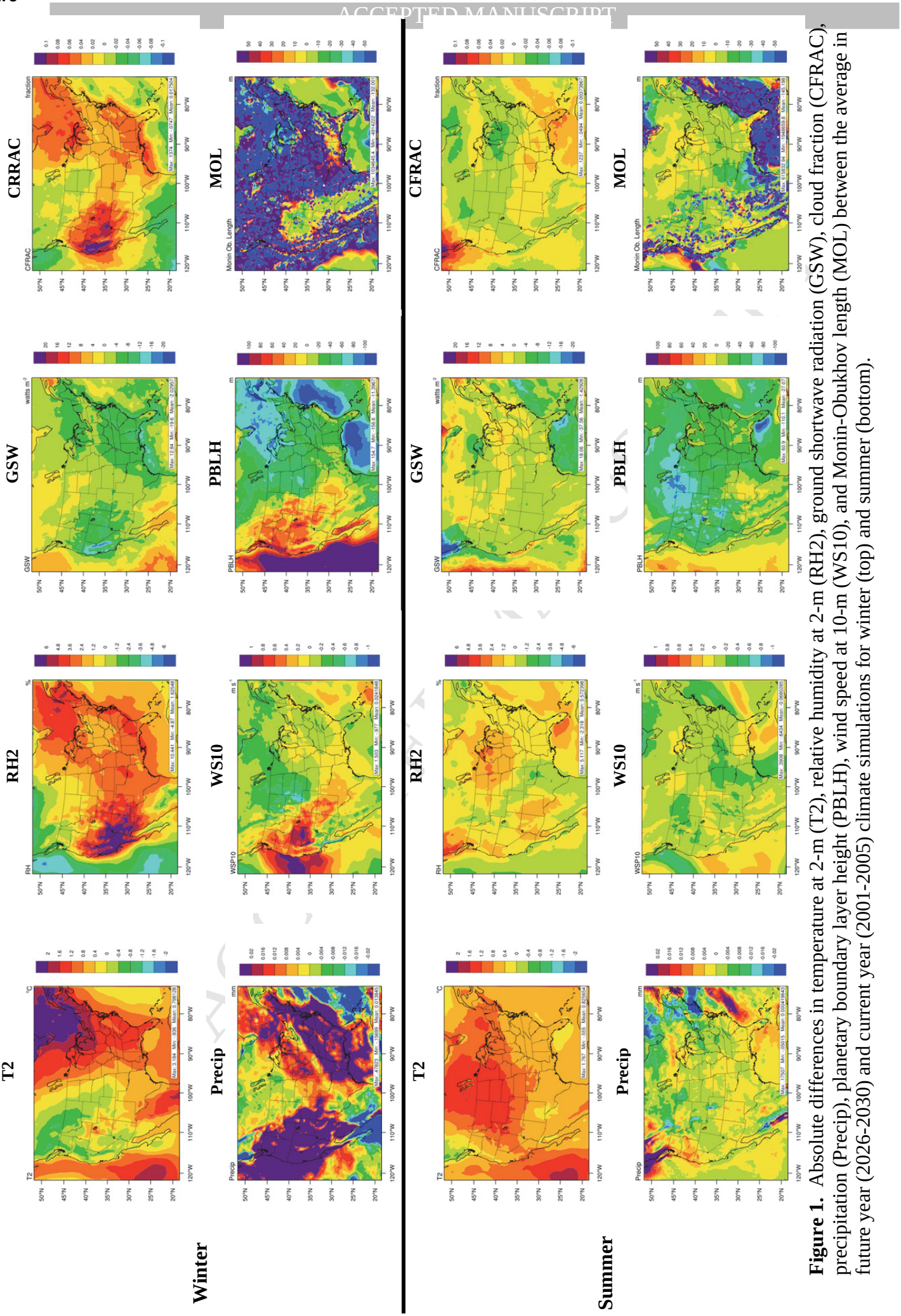

Figure 1. Absolute differences in temperature at 2-m (T2), relative humidity at 2-m (RH2), ground shortwave radiation (GSW), cloud fraction (CFRAC), precipitation (Precip), planetary boundary layer height (PBLH), wind speed at 10-m (WS10), and Monin-Obukhov length (MOL) between the average in future year (2026-2030) and current year (2001-2005) climate simulations for winter (top) and summer (bottom).

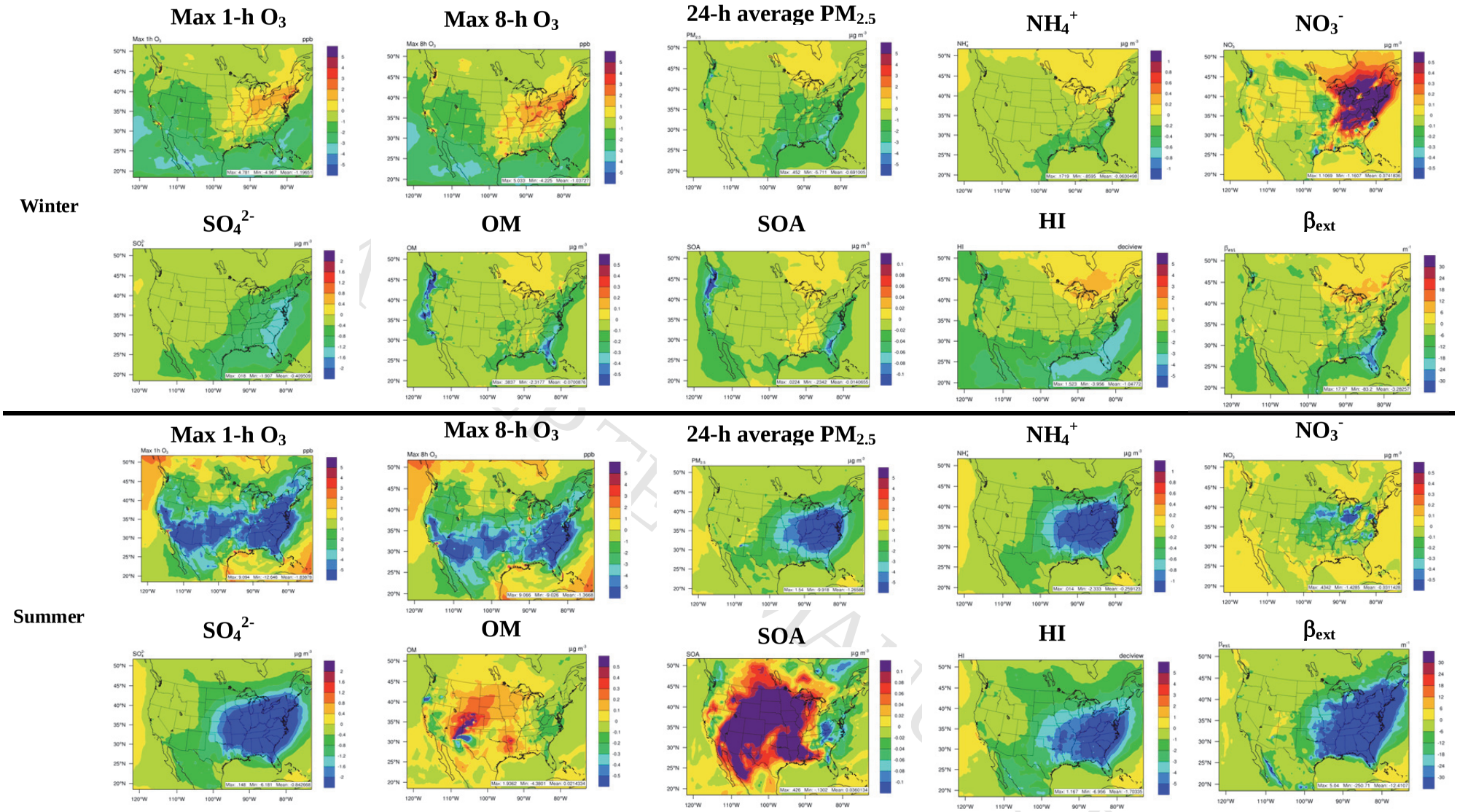

Figure 2. Absolute differences in mixing ratios of maximum 1-h average O_3, maximum 8-h average O_3, concentrations of $PM_{2.5}$, NH_4^+, NO_3^-, SO_4^{2-}, OM, and SOA, and visibility parameters, HI and β_{ext}, between the average future year (2026-2030) and current year (2001-2005) air quality simulations for winter (top) and summer (bottom).

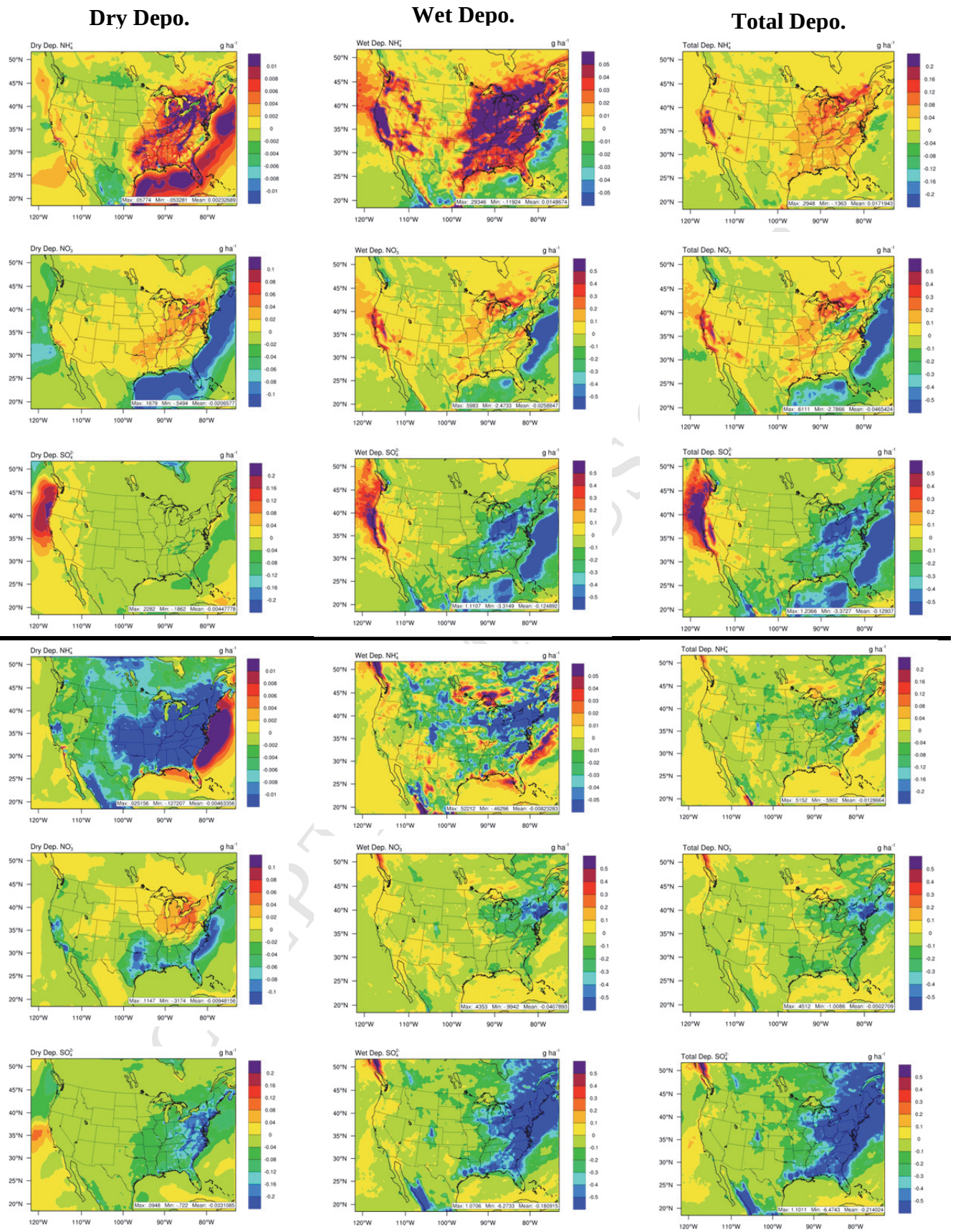

Figure 3. Absolute differences in dry, wet, and total deposition fluxes of NH_4^+, NO_3^-, and SO_4^{2-} for winter (top) and summer (bottom).

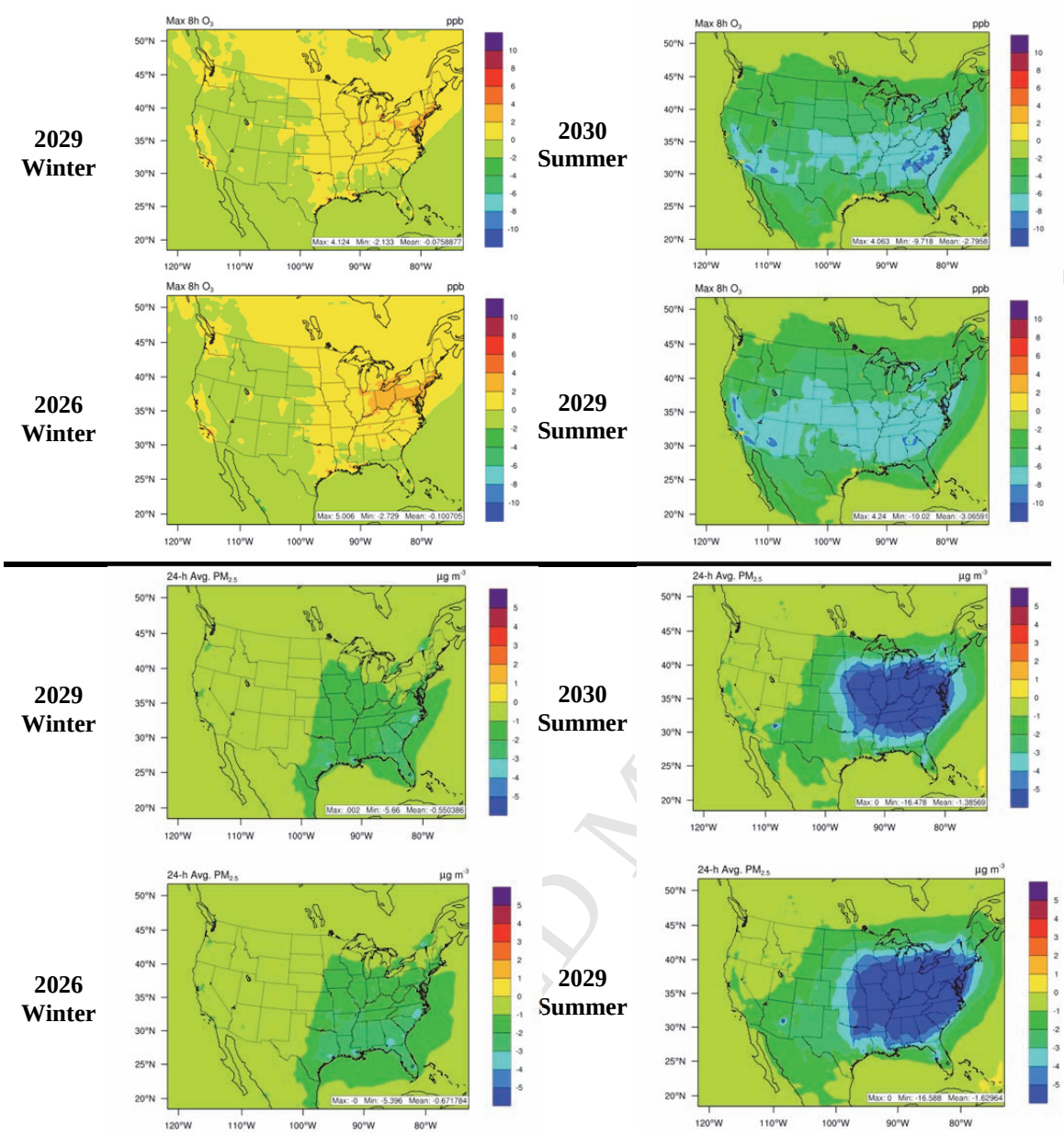

Figure 4. Contributions of projected anthropogenic emissions to maximum 8-h average O_3 (top) and $PM_{2.5}$ (bottom) during future winter with potentially good and poor air quality (2029 and 2026, respectively) and future summers with potentially good and poor air quality (2030 and 2029, respectively).

Supplementary Material

Impacts of Future Climate and Emission Changes on U.S. Air Quality

Ashley Penrod[a], Yang Zhang[a,*], Kai Wang[a], Shiang-Yuh Wu[b], and L. Ruby Leung[c]

[a]Department of Marine, Earth, and Atmospheric Sciences, North Carolina State University, Raleigh, North Carolina, USA.

[b]Department of Air Quality and Environmental Management, Clark County, Nevada, USA.

[c]Pacific Northwest National Laboratory, Richland, Washington, USA.

[*]Corresponding author: Yang Zhang, Department of MEAS, NCSU, Campus Box 8208, Raleigh, NC 27695-8208, USA. Tel: 919 515 9688; fax: 919 515 7802. Email address: yang_zhang@ncsu.edu

1. Model configurations

Table S1 shows the model configurations including physics and chemical options. The Carbon-Bond Mechanism (CB05) is used to simulate gas-phase chemistry while AERO6 is used as the aerosol module with the thermodynamic equilibrium model ISORROPIA v2.0 that accounts for the effects of crustal species on aerosol thermodynamic equilibrium (Fountoukis and Nenes, 2007). CMAQ v5.0 includes a number of improved treatments, such as the simulation of O_3 in urban plumes in the updated toluene chemistry of the CB05 mechanism, additional PM speciation for primary PM emissions, improved gas/particle partitioning of inorganic species and elimination/moderation of numerical instabilities in ISORROPIA version 2.0, updated secondary organic aerosol yield parameterization, and updated vertical diffusion and advection algorithms. New treatments that are not available in previous versions include primary organic aerosol aging by OH radicals as a second-order reaction, in-line calculated photolysis rates, in-line calculated biogenic emissions and wind-blown dust emissions, and in-line or off-

line nitric oxide (NO) emissions from lightning. In this work, the inline wind-blown dust emission module and the module for NO emissions from lightning are not activated, due to the unavailability of input files at the time of the beta version release. Omission of such emissions may contribute to some of the model biases in simulating relevant species such as NO_x, O_3, and PM_{10}. A lookup table of actinic flux is used for photolysis rates instead of the in-line option, as O_3 column data needed for the in-line option is not available for future years. In addition, in the CMAQ v5.0 beta version, the treatment of bi-directional flux of ammonia (NH_3) is based on CMAQ v4.7, which is used in this work. In the publically-released CMAQ v5.0, several updates were made including updated parameterizations based on published field scale models and NH_3 exchanges based on varying land use, soil, and plant compensation points. While the updated treatments of advection and the stable the planetary boundary layer (PBL) in the publically-released version affect column mass slightly, differences between the results with the publically-released version and the beta version are very small.

2. Emissions for current and future year simulations

Criteria and hazardous air pollutant emission inventories and ancillary files for current year simulations are based on the U.S. EPA's 2002 National Emissions Inventory (NEI), while biogenic emissions for both current and future year scenarios are processed in-line with CMAQ v5.0 and are based on the Biogenic Emissions Inventory System (BEIS) version 3.13. Emissions of wind-blown dust and NO from lightning are not included for the reason stated previously. Raw anthropogenic emission inventories are spatially allocated, chemically speciated, and temporally allocated using the Sparse Matrix Operator Kernel Emissions (SMOKE) modeling system version 2.6 to match the temporal, horizontal, and vertical resolutions of CMAQ. The input emissions for the latest version of CMAQ (v5.0) require additional speciation of unspeciated fine particulate matter (PMOTHR) that is not included in previous versions of

CMAQ. The speciation of PMOTHR in this work is based on that of Reff et al. (2009), namely, PMOTHR is split into 14 particulate species: water, noncarbon organic matter, sodium, aluminum, calcium, iron, silicon, chloride, potassium, ammonium, titanium, manganese, magnesium, and other, which includes all unaccounted minor trace elements, metal bound oxygen, and other unspeciated $PM_{2.5}$. Domain-wide speciated growth factors for future (2026-2030) anthropogenic emissions are applied to the base 2002 NEI speciated, model-ready, and gridded emissions outside of SMOKE. The future-year simulations are based on the IPCC SRES A1B scenario, which is characterized by rapid economic growth, moderate population growth that peaks in 2050 and declines thereafter, and rapid growth and introduction of new, more energy efficient technologies, with a balance across all energy sectors (IPCC, 2000). The IMAGE model developed by the National Institute for Public Health and the Environment (RIVM) in the Netherlands (RIVM, 2001) is used to disaggregate the A1B scenario into additional pollutant emissions. Table S2 shows the lumped growth factors (GFs) for the A1B scenario that are derived based on GFs for 8 source sectors over the U.S. developed by Argonne National Laboratory (ANL) (personal communications, David Streets, ANL, 2011) following the approach of Nakicenovic et al. (2000) and RIVM (2001). The emissions of formaldehyde, ammonia, and nitrate are projected to increase (i.e., with a GF > 1) by 2030, while those of anthropogenic volatile organic compounds (VOCs), NO_x, EC, primary organic carbon, fine particulate matter, sulfur dioxide (SO_2), and others are projected to decrease (i.e., with a GF < 1). Propinaldehyde and higher aldehydes are not included in the original ANL growth factors, whose GFs are assumed to be the same as acetaldehyde. These growth factors are applied to the gridded 2002 NEI emissions to produce the gridded future year emissions inventory.

3. Observational datasets

Table S3 shows observational datasets used in the evaluation of the WRF/CMAQ simulations along with meteorological variables and chemical concentrations evaluated, their data frequency and total number of sites. Surface-based observations are obtained from nine monitoring networks: the Clean Air Status and Trends Network (CASTNET), the Aerometric Information Retrieval System-Air Quality System (AIRS-AQS), the Interagency Monitoring of Protected Visual Environments (IMPROVE), the Chemical Speciation Network (CSN), the Southeastern Aerosol Research and Characterization study (SEARCH), the North Carolina Department of Environment and Natural Resources (NCDENR), and the National Acid Deposition Program (NADP). Satellite measurements include tropospheric CO column abundances from the Measurements of Pollution in the Troposphere (MOPITT), tropospheric NO_2 and HCHO column abundances from the Global Ozone Monitoring Experiment (GOME), tropospheric O_3 residuals (TORs) derived from the Total Ozone Monitoring Experiment (TOMS) and the Solar Backscattered Ultraviolet (SBUV), and aerosol optical depths (AODs) from the Moderate Resolution Imaging Spectroradiometer (MODIS). Meteorological variables (i.e., temperature and pressure) and layer thickness from MCIP outputs are used in conjunction with CMAQ simulated mass concentrations to calculate and convert column abundances of CO, NO_2, HCHO, and O_3 into Dobson Unit (DU) for O_3, and molecules cm^{-2} for other species. Total (fine- and coarse-mode) MODIS-derived AODs are compared with the calculated AOD based on the parameterizations of Zhang et al. (2009) using fine and coarse PM predicted by CMAQ, layer thickness, and the total number of layers.

4. Evaluation of the 2002 WRF_NCEP/CMAQ simulations

Figure S1 shows the spatial distribution of NMBs of maximum 8-h O_3 mixing ratios and $PM_{2.5}$ concentrations at the AIRS-AQS, CASTNET, and SEARCH sites. Spatially, overpredictions in maximum 8-h O_3 mixing ratios occur at the AIR-AQS sites in the southeast particularly along the Gulf coast, California, and parts of the Midwest in both seasons and at the SEARCH sites during summer. The maximum 8-h O_3 mixing ratios are generally underpredicted at the CASTNET sites (mostly rural/remote sites), with the largest overpredictions in the states of Washington, Florida, and West Virginia in both seasons. These results are similar to Appel et al. (2007), who reported a slight overprediction to unbiased performance for O_3 over the eastern U.S. in summer with CMAQ v4.5, with an overprediction in the winter as well. Appel et al. (2011b) also reported an overprediction of daytime O_3 mixing ratios over North America (an NMB of 9.7%), but found that winter O_3 mixing ratios were greatly underpredicted when using the Global and regional Earth-system Monitoring using Satellite and in-situ data (GEMS) as lateral boundary conditions. The underprediction of O_3 in winter reported by Appel et al. (2011) was not evident when the simulations were conducted with chemical boundary conditions from GEOS-Chem.

Discrepancies between model predictions and observations in this work for O_3 may be due to uncertainties in the emissions of precursors (e.g., nitrogen oxides (NO_x = NO + NO_2) and volatile organic compounds (VOCs)) (Wang and Zhang, 2012). As shown in Table 3, the mixing ratios of NO, one of the precursors for O_3, are underpredicted at the SEARCH sites in summer and winter, leading to overpredicted O_3 at SEARCH sites due mainly to insufficient titration. The discrepancies between simulated and observed O_3 mixing ratios may also be due to

inaccuracies in meteorological variables that affect chemical concentrations. For example, overpredictions in WS10 can lead to underpredictions in O_3 mixing ratios at the source and overpredictions downwind, and underpredictions in T2 can lead to underpredictions in O_3 mixing ratios due to a weaker photochemistry than it should be. The inaccuracies in the simulated PBLH may also lead to biases in O_3 predictions. No observations are available for PBLH evaluation. However, the model performance for CO, a relatively long-lived, slowly reactive species, may provide an indicator to some extent to assess the model's capability in representing PBLH and thus vertical mixing (Zhang et al., 2013). As shown in Table 3, CO mixing ratios at the SEARCH sites are underpredicted. While this underprediction may be caused by several factors (e.g., an underestimate of CO emissions and an overestimate in dry deposition), one possible factor is an overestimate of simulated PBLH, which increases mixing and leads to underpredictions of CO, NO, and HNO_3 at the SEARCH sites. One reason for the bias of PBL height may be the vertical resolution used in this study, which has been found to affect PBL height predictions (Hanna and Yang, 2001). In addition to the possible bias in PBLH, the underpredictions in NO_x emissions may be one main reason for large underpredictions of NO and HNO_3 at the SEARCH sites. Finally, the grid resolution of 36-km is too coarse to capture meteorological phenomena and chemistry at fine- or meso- scales.

As shown in Figure S1, CMAQ generally overpredicts the concentrations of $PM_{2.5}$ and its components in winter while underpredicting them in summer, with a few exceptions (e.g., NO_3^-, OC, and total carbon (TC) at the CSN sites and OC and TC at the IMPROVE sites in winter, SO_4^{2-}, NO_3^-, and NH_4^+ at the SEARCH sites and EC at the CSN sites in summer). At the SEARCH sites, SO_4^{2-}, NO_3^-, and NH_4^+ concentrations are significantly overpredicted in summer

(NMBs of 165.5, 98.0, 199.0%, respectively), with the SO_4^{2-} overprediction due possibly to several factors such as an overestimation of SO_2 emissions from other non-EGU sources, uncertainties in the vertical distributions of SO_2 emissions, and uncertainties in dry/wet deposition and aqueous-phase chemistry treatments at the SEARCH sites. Predictions at the CASTNET sites for SO_4^{2-}, NO_3^-, and NH_4^+ are good to moderately good in both seasons with NMBs of -33.9% to 30.5%, with the exception of SO_4^{2-} in winter (an NMB of 44.3%). Large model biases occur for some species at some sites e.g., the NO_3^- at the SEARCH sites in both seasons and at the IMPROVE sites in summer (NMBs of -79.2% to 98% and -46.4%), NH_4^+ at the IMPROVE sites in winter and at the SEARCH sites in summer (NMBs of 59% and 199%, respectively), SO_4^{2-} at all sites in winter and at SEARCH sites in summer (NMBs of 36.4-159.2% and 165.5%, respectively), and OC at the IMPROVE sites in summer (an NMB of -60.1%). The seasonal performance of those species at the remaining sites is good to marginally good with NMBs of -29.3% to -21.3% for summer SO_4^{2-}, -6.8% to 34.7% and -33.9% to -27.9% for winter and summer NO_3^-, 17.9-30.5% and -26.5 to -11.9% for winter and summer NH_4^+, respectively, 1.3-13.2% and -18.6% to 1.2% for winter and summer EC, respectively, and -11.2% for winter OC.

Discrepancies between observed and simulated $PM_{2.5}$ and its components may be due to a number of factors. First, uncertainties exist in the emissions of gaseous precursors of secondary $PM_{2.5}$, as well as primary $PM_{2.5}$ (OC and EC). For example, underestimation of $PM_{2.5}$, OC, and TC concentrations in summer may be due to coarse spatial and temporal distributions of wildfire emissions (Roy et al., 2007) and the exclusion of dust emissions. Uncertainties in the emissions of gaseous precursors such as NH_3 in the 2002 NEI and previous versions may contribute to

biases in NO_3^- and NH_4^+ (Pinder el al., 2006; Zhang et al., 2006 a, b; S.-Y. Wu et al., 2008; Wang and Zhang, 2012). The overpredictions in the concentrations of SO_2 and SO_4^{2-} at the CASTNET sites in winter may be due in part to overpredictions of SO_2 emissions. Second, uncertainties exist in the model parameters used such as the rate constant and heterogeneous reaction probability, γ, used in simulating the heterogeneous reactions of NO_2 and N_2O_5 to produce HNO_3. This uncertainty may help explain the overpredictions in the concentrations of HNO_3 and NO_3^- during winter. CMAQ v5.0 includes the heterogeneous reactions of $NO_2 + H_2O$ and $N_2O_5 + H_2O$ that contribute to HNO_3 production. The $NO_2 + H_2O$ reaction is assumed to occur on the surfaces of aerosol and the ground surface areas with a rate constant of 3.0×10^{-3} S/V m^{-1} (S/V is the ratio of surface area to volume of air) (Sarwar et al., 2008). The N_2O_5 heterogeneous reaction probability, γ, is calculated as a function of temperature, relative humidity, particle composition, and phase state following the parameterization of Davis et al. (2008). The heterogeneous reaction of N_2O_5 and NO_2 may be the most important pathway to produce HNO_3 during the winter time. However, the rate constant of $NO_2 + H_2O$ and the γ parameterization of N_2O_5 used have not been evaluated with ambient measurements during winter time due to the lack of observations. In particular, while the γ parameterization of N_2O_5 used in CMAQ v5.0 may reproduce the ambient measurements, it remains unclear if this parameterization can reproduce observed concentrations during winter months because the underlying steady state approximation is not applicable at cold temperatures (Brown et al., 2003; Davis et al., 2008). Third, model representations of gas/particle partitioning, dry deposition, and scavenging/wet deposition fluxes may add to biases of the PM predictions (Wang and Zhang, 2012). For example, the underprediction in dry and wet deposition fluxes of SO_2, SO_4^{2-}, NO_3^-,

and NH_4^+ in winter may be a factor in the overprediction of SO_2, SO_4^{2-}, NO_3^-, and NH_4^+ in winter (with the exception of NO_3^- at the CSN sites). Fourth, the spatial variability and biases of meteorology can affect predictions of $PM_{2.5}$ and its components. Overpredictions of WS10, PBLH, and precipitation can lead to underpredictions of PM concentrations in summer due to increased dispersion, ventilation, and precipitation scavenging. For example, the underprediction of Precip in winter could be a factor in the overprediction of SO_2, $PM_{2.5}$, and $PM_{2.5}$ inorganic components due to decreased scavenging. Compared to winter, larger underprediction occurs in Precip, which may lead to underpredictions in aqueous-phase oxidation rates of SO_2 thus the concentrations of SO_4^{2-}. Finally, the use of a coarse grid resolution also contributes to the model biases in simulated PM and its composition. The model evaluation results are generally consistent with those reported by other studies (Zhang et al., 2008, 2009; Appel et al., 2011; Wang and Zhang, 2012). It is important to note that there are differences among model setups that affect model performance, such as differences in emission inventories, meteorological models and their predictions (specifically precipitation), air quality models and versions, the grid resolution, years of simulation, and observations used for model evaluation.

Figure S2 shows the observed and simulated seasonal average spatial distributions of tropospheric column abundances of CO, NO_2, HCHO, TOR, and AOD in winter and summer 2002 from CMAQ simulations driven by meteorological predictions from WRF_NCEP. The MOPITT-derived CO column abundance is high over the eastern and western U.S. coasts, but is generally underpredicted by CMAQ in these regions, with better agreement over high altitude regions in winter, specifically over the Rocky Mountains. In terms of seasonal statistical

performance, CMAQ predicts CO columns fairly well, with better results in winter compared to summer (NMBs of -8.1% and -17.0%, respectively). Discrepancies between the prediction and observations could be due to uncertainties in CO emissions, MOPITT retrieval methods, and boundary conditions (Emmons et al., 2009; Wang and Zhang, 2012). Spatially, CMAQ produces well column NO_2 in summer and winter, but overpredicts in high populated regions and major cities such as Chicago, IL, New Orleans, LA, Houston, TX, and Seattle, WA. Statistically, CMAQ overpredicts column NO_2, particularly in winter with an NMB of 43.4%, likely due to uncertainties in the NO_2 emissions, boundary conditions, and NO_2 oxidation rates in the CB05 gas-phase mechanism (Wang and Zhang, 2012).

The performance of CMAQ at capturing HCHO columns is overall poor, both spatially and statistically. In general, CMAQ underpredicts the HCHO columns in winter (an NMB of -26.5%) and overpredicts them in summer (an NMB of 52.0%). Discrepancies between the GOME and CMAQ HCHO columns may be due to large uncertainties associated with satellite retrieval methods, high yields of HCHO from the oxidation of BVOCs in the CB05 chemical mechanism of CMAQ, and uncertainties in HCHO emissions (Wang and Zhang, 2012). CMAQ does not capture the spatial distribution of TOR, particularly in the summer, with large underpredictions over the southeastern U.S. and the California coast. Winter TOR is better captured by CMAQ, both spatially and statistically, with an NMB of 11.3%. Discrepancies of modeled and TOMS/SBUV O_3 may be due to the boundary conditions of O_3 provided by GEOS-Chem (Wang et al., 2009). The seasonal variation of CMAQ-derived and MODIS AOD is evident, with lower AODs in the winter. CMAQ-derived AODs are underpredicted domain-wide in both summer and winter (NMBs of -37.0 and -41.8%, respectively), with the exception of the

southeastern and northeastern U.S. in winter. Several factors may explain the differences between MODIS and CMAQ-derived AODs. First, the CMAQ simulations in this study do not consider windblown dust (which may contribute to the derived AODs), whereas it is accounted for in the total MODIS AOD (Wang and Zhang, 2012). Second, underpredictions of surface concentrations of OC in winter and summer and SO_4^{2-}, NO_3^-, and NH_4^+ in summer (with the exception of the SEARCH sites), may contribute to the underprediction of CMAQ-derived AODs in summer and winter. Finally, uncertainties exist in a number of parameters used to calculate the CMAQ AODs as well as the MODIS data (Drury et al., 2008; Wang and Zhang, 2012).

References

Appel, K. W., Gilliland, A. B., Sarwar, G., Gilliam R. C., 2007. Evaluation of the Community Multiscale Air Quality (CMAQ) model version 4.5: Sensitivities impacting model performance Part I - Ozone. Atmospheric Environment 41(40), 9603-9615, doi:10.1016/j.atmosenv.2007.08.044.

Appel, K. W., Roselle, S. J., Pleim, J., Mathur, R., 2011. Evaluation of CMAQ v5.0 Performance for January and July 2006, 10th Annual CMAS Conference, Chapel Hill, NC.

Davis, J.M., Bhave, P.V., Foley K.M., 2008. Parameterization of N_2O_5 reaction probabilities on the surface of particles containing ammonium, sulfate, and nitrate. Atmospheric Chemistry and Physics 8, 5295–5311.

Drury, E., Jacob, D. J., Wang, J., Spurr, R. J. D., Chance, K., 2008. Improved algorithm for MODIS satellite retrievals of aerosol optical depths over western North America. Journal of Geophysical Research 113(D16), D16204, doi:10.1029/2007JD009573.

Emmons, L. K., Edwards, D. P., Deeter, M. N., Gille, J. C., Campos, T., Nedelec, P., Novelli, P., Sachse, G., 2009. Measurements of Pollution In The Troposphere (MOPITT) validation through 2006. Atmospheric Chemistry and Physics 9(5), 1795-1803.

Fountoukis, C., Nenes, A., 2007. ISORROPIA II: a computationally efficient thermodynamic equilibrium model for K^+-Ca^{2+}-Mg^{2+}-NH_4^+-Na+-SO_4^{2-}-NO_3^--Cl^--H_2O aerosols. Atmospheric Chemistry and Physics 7(17), 4639-4659.

Hanna, S., Yang, R., 2001. Evaluations of mesoscale models' simulations of near-surface winds, temperature gradients, and mixing depths. Journal of Applied Meteorology 40(6), 1095-1104, doi:10.1175/1520-0450(2001)040<1095:EOMMSO>2.0.CO;2.

Nakicenovic, N., Davidson, O., Davis, G., Grubler, A., Kram, T., La Rovere, E. L., Metz, B., Morita, T., Pepper, W., Pitcher, H., Sankovski, A., Shukla, P., Swart, R., Watson, R., Dadi, Z., 2000. Emissions Scenarios: A Special Report of Working Group III of the Intergovernmental Panel on Climate Change. Cambridge University Press, New York, N.Y.

Pinder, R. W., Adams, P. J., Pandis, S. N., Gilliland, A. B., 2006. Temporally resolved ammonia emission inventories: Current estimates, evaluation tools, and measurement needs.Journal of Geophysical Research 111(D16), D16310, doi:10.1029/2005JD006603.

Reff, A., Bhave, P. V, Simon, H., Pace, T. G., Pouliot, G. A., Mobley, J. D., Houyoux, M., 2009. Emissions Inventory of $PM_{2.5}$ Trace Elements across the United States. Environmental Science & Technology 43(15), 5790-5796, doi:10.1021/es802930x.

RIVM (National Institute for Public Health and the Environment), 2001. The IMAGE 2.2 Implementation of the SRES Scenarios: A Comprehensive Analysis of Emissions, Climate Change and Impacts in the 21st Century (CD-ROM). RIVM Publication. 481508018, Bilthoven, Netherlands, July.

Roy, B., Pouliot, G. A., Gilliland, A., Pierce, T., Howard, S., Bhave, P. V., Benjey, W., 2007. Refining fire emissions for air quality modeling with remotely sensed fire counts: A wildfire case study. Atmospheric Environment 41(3), 655-665, doi:10.1016/j.atmosenv.2006.08.037.

Sarwar, G., Roselle, S.J., Mathur, R., Appel, W., Dennis, R.L., Vogel, B., 2008. A comparison of CMAQ HONO predictions with observations from the Northeast Oxidant and Particle Study. Atmospheric Environment 42, 5760–5770.

Wang, K., Zhang, Y., Jang, C., Phillips, S., Wang, B., 2009. Modeling intercontinental air pollution transport over the trans-Pacific region in 2001 using the Community Multiscale Air Quality modeling system. Journal of Geophysical Research 114, D04307, doi:10.1029/2008JD010807.

Wang, K., Zhang, Y., 2012. Application Evaluation, and Process Analysis of the US EPA's 2002 Multiple-Pollutant Air Quality Modeling Platform. Atmos. Clim. Sci., 2, 254-289, doi:10.4236/acs.2012.23025.

Wu, S.-Y., Krishnan, S., Zhang, Y., Aneja, V., 2008. Modeling atmospheric transport and fate of ammonia in North Carolina - Part I: Evaluation of meteorological and chemical predictions. Atmospheric Environment 42(14), 3419-3436, doi:10.1016/j.atmosenv.2007.04.031.

Zhang, Y., Liu, P., Queen, A., Misenis, C., Pun, B., Seigneur, C., Wu, S.-Y., 2006a. A comprehensive performance evaluation of MM5-CMAQ for the summer 1999 Southern oxidants study episode-Part II: Gas and aerosol predictions. Atmospheric Environment 40(26), 4839-4855, doi:10.1016/j.atmosenv.2005.12.048.

Zhang, Y., Liu, P., Pun, B., Seigneur, C., 2006b. A comprehensive performance evaluation of MM5-CMAQ for the summer 1999 southern oxidants study episode, Part III: Diagnostic and mechanistic evaluations. Atmospheric Environment 40(26), 4856-4873, doi:10.1016/j.atmonsenv.2005.12.046.

Zhang, Y., Hu, X., Leung, L. R., W. I. Gustafson Jr., 2008. Impacts of regional climate change on biogenic emissions and air quality. Journal of Geophysical Research 113(D18), D18310, doi:10.1029/2008JD009965.

Zhang, Y., Vijayaraghavan, K., Wen, X., Snell, H. E., Jacobson, M. Z., 2009. Probing into regional ozone and particulate matter pollution in the United States: 1. A 1 year CMAQ simulation and evaluation using surface and satellite data. Journal of Geophysical Research 114, D22304, doi:10.1029/2009JD011898.

Zhang, Y., Olsen, K., Wang, K., 2013. Fine Scale Modeling of Agricultural Air Quality over the Southeastern United States using Two Air Quality Models, Part I. Application and Evaluation. Aerosol and Air Quality Research, 13 (4): 1231–1252.

Table S1. Model components and configurations

Attribute	Configuration
Simulation Period	Summer (June, July, August) and winter (December, January, February) of 2001-2005 and 2026-2030
Domain	Continental U.S.
Horizontal resolution	36 km
Vertical resolution	14 layers from the surface to about 15 km (~100 mb)
Meteorological IC and BC	NCEP-Final (NCEP-FNL) Operational Global Analysis data for WRF_NCEP simulations and Community Climate System Model data for WRF_CCSM simulations
Shortwave and longwave radiation	Community Atmosphere Model
Land surface	Soil thermal diffusion
Surface layer	Monin-Obukhov
PBL	Yonsei University scheme
Cumulus	Kain-Fritsch
Microphysics	WRF single-moment 6-class graupel
Gas-phase chemistry	2005 Carbon-Bond Mechanism (CB05)
Aqueous-phase chemistry	Modified RADM mechanism
Aerosol module	Aerosol module version 6
Chemical IC and BC	Goddard Earth Observing System Model with Chemistry (GEOS-Chem)
Anthropogenic emissions	2002 National Emissions Inventory
Biogenic emission	Biogenic Emissions Inventory System version 3.13

Table S2
Domain-uniform lumped growth factors for anthropogenic species

Emitted Species	Growth Factor
Acetaldehyde	0.93
Carbon monoxide	0.62
Ethene	0.59
Ethane	0.89
Formaldehyde	1.14
Internal olefin carbon bond	0.96
Ammonia	1.34
Nitrous oxide	0.72
Nitrogen dioxide	0.72
Terminal olefin carbon bond	0.96
Paraffin carbon bond	0.90
Elemental carbon[a]	0.65
Primary coarse particulate matter [a]	0.95
Other inorganic fine particulate matter[a]	0.79
Nitrate[a]	1.01
Primary organic carbon[a]	0.91
Sulfate[a]	0.81
Sulfur dioxide	0.25
Toluene and other monoalkyl aromatics	0.66
Xylene and other polyalkyl aromatics	0.56

[a]Particulate species

Table S3
Surface and satellite databases used for model evaluation

Database[a]	Variable(s) Evaluated[b]	Data Frequency	Number of Sites
CASTNET	T2, WS10, RH2, O_3, SO_2, HNO_3, NO_3^-, NH_4^+, SO_4^{2-}	Hourly met. and O_3; Weekly average PM components	~80 sites, in remote/rural areas of the U.S.
CSN	T2, $PM_{2.5}$, NO_3^-, NH_4^+, SO_4^{2-}, EC, OC, TC	24-h average, 1 every 3 days	~130 sites, in urban areas of the U.S.
NADP	Precip, wet dep. of NH_4^+, SO_4^{2-}, NO_3^-	Weekly total	Over 250 sites, nationwide
SEARCH	T2, WS10, RH2, O_3, CO, NO, SO_2, HNO_3, $PM_{2.5}$, NO_3^-, NH_4^+, SO_4^{2-}	Hourly	8 sties, in the urban/suburban areas of the southeastern U.S.
AIRS-AQS	O_3	Hourly	Over 1100 sites, mostly in cities and towns in the U.S.
IMPROVE	$PM_{2.5}$, NO_3^-, NH_4^+, SO_4^{2-}, EC, OC, TC, β_{ext}, HI	24-h average, 1 every 3 days	~130 sites, primarily in remote locations in the western U.S.
NCDENR	O_3, $PM_{2.5}$, NH_3	Hourly	8 sites for $PM_{2.5}$, 3 sites for NH_3, in North Carolina
GOME	Column NO_2, HCHO	Monthly average	Domain-wide
MODIS	AOD	Monthly average	Domain-wide
MOPITT	Column CO	Monthly average	Domain-wide
TOMS/SBUV	TOR	Monthly average	Domain-wide

[a]CASTNET, Clean Air Status and Trends Network (http://www.epa.gov/castnet); CSN, Chemical Speciation Network (http://www.epa.gov/ttnamti1/speciepg.html); NCAR-RDA, National Center of Atmospheric Research-Research and Data Archive ds472.0 (http://rda.ucar.edu/datasets/ds472.0/); NADP, National Acid Deposition Program (http://nadp.sws.uiuc.edu); SEARCH, Southeastern Aerosol Research and Characterization (http://www.atmospheric-research.com/studies/SEARCH/index.html); MADIS, Meteorological Assimilation Data Ingest System (http://madis.noaa.gov); AIRS-AQS, Aerometric Information Retrieval System-Air Quality Subsystem (http://www.epa.gov/air/data/index.html); IMPROVE, Interagency Monitoring of Protected Visual Environments (http://vista.cira.colostate.edu/improve); NCDENR, North Carolina Department of Environment and Natural Resources (http://daq.state.nc.us/monitor); GOME, Global Ozone Monitoring Experiment (http://wdc.dlr.de/data_products/); MODIS, Moderate Resolution Imaging Spectroradiometer (http://ladsweb.nascom.nasa.gov); MOPITT, Measurements of Pollution in the Troposphere (http://eosweb.larc.nasa.gov/PRODOCS/mopitt/table_mopitt.html); TOMS/SBUV, Total Ozone Mapping Spectrometer and the Solar Backscattered Ultraviolet (http://ozoneaq.gsfc.nasa.gov/measurements.md).
[b]β_{ext}, extinction coefficient; HI, Haziness Index.

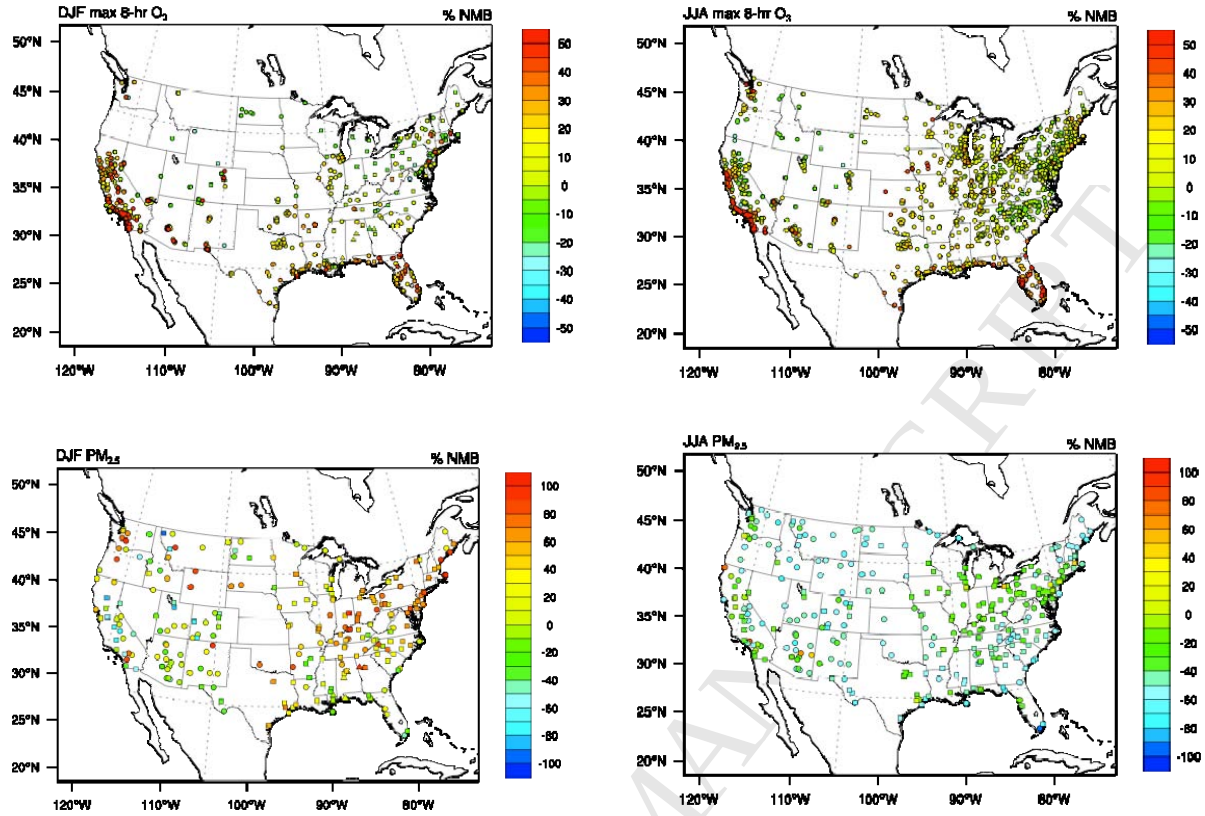

Figure S1. Spatial distributions of NMBs of maximum 8-h average O_3 and 24-h average $PM_{2.5}$ predictions over the U.S. in winter (DJF) and summer (JJA) in 2002. The observational datasets for maximum 8-h average O_3 include AIRS-AQS (circles), CASTNET (square), and SEARCH (triangle) and IMPROVE (circle), SEARCH (triangle), and CSN (square) for 24-h average $PM_{2.5}$.